Improving Multisensor Estimation of Heavy-to-Extreme Precipitation via Conditional Bias-Penalized Optimal Estimation

Beomgeun Kim[1,*], Dong-Jun Seo[1], Seong Jin Noh[1], Olivier P. Prat[2], Brian R. Nelson[3]

Deptment of Civil Engineering, the University of Texas at Arlington, Arlington, TX, USA

Cooperative Institute for Climate and Satellites and NOAA/NCEI, Asheville, NC, USA

Remote Sensing Applications Division, NOAA/NCEI, Asheville, NC, USA

Corresponding author: Beomgeun Kim (kbg0201@gmail.com)

Submitted to

Special Issue on Precipitation measurement and modeling: uncertainty, variability, observations, ensemble simulation and downscaling

Journal of Hydrology

Abstract

A new technique for merging radar precipitation estimates and rain gauge data is developed and evaluated to improve multisensor quantitative precipitation estimation (QPE), in particular, of heavy-to-extreme precipitation. Unlike the conventional cokriging methods which are susceptible to conditional bias (CB), the proposed technique, referred to herein as conditional bias-penalized cokriging (CBPCK), explicitly minimizes Type-II CB for improved quantitative estimation of heavy-to-extreme precipitation. CBPCK is a bivariate version of extended conditional bias-penalized kriging (ECBPK) developed for gauge-only analysis. To evaluate CBPCK, cross validation and visual examination are carried out using multi-year hourly radar and gauge data in the North Central Texas region in which CBPCK is compared with the variant of the ordinary co-kriging (OCK) algorithm used operationally in the National Weather Service Multisensor Precipitation Estimator. The results show that CBPCK significantly reduces Type-II CB for estimation of heavy-to-extreme precipitation, and that the margin of improvement over OCK is larger in areas of higher fractional coverage (FC) of precipitation. When FC > 0.9 and hourly gauge precipitation is greater than 60 mm, the reduction in root mean squared error (RMSE) by CBPCK over radar-only (RO) is about 12 mm while the reduction in RMSE by OCK over RO is about 7 mm. CBPCK may be used in real-time analysis or in reanalysis of multisensor precipitation for which accurate estimation of heavy-to-extreme precipitation is of particular importance.

Key words: multisensor quantitative precipitation estimation, radar precipitation, rain gauges, conditional bias, cokriging

1. Introduction

Heavy-to-extreme rainfall is a growing concern in many parts of the world since it is often a direct cause for serious natural disasters such as flash floods, urban inundation, river floods and landslides. For high-resolution precipitation estimation, many techniques based on weather radar have been investigated and developed over the last 60 years (Chandrasekar et al., 2013; Chen and Chandrasekar, 2015; Gourley et al., 2009; Kitzmiller et al., 2011; Marshall et al., 1955; Nelson et al., 2015; Vasiloff et al., 2007; Westrick et al., 1999; Yamaguchi et al., 2012; Young et al., 2000; Zhang et al., 2012; Zhang et al., 2011). Examples of the most recent advances and challenges in hydrologic applications of weather radar can be found in Seo et al. (2015) and references therein. Radar quantitative precipitation estimation (QPE), however, is subject to various error sources such as uncertain Z-R relationships, lack of calibration, attenuation, anomalous propagation (AP) and nonuniform vertical profile of reflectivity (VPR), etc. (Austin, 1987; Fang et al., 2004; Smith et al., 1996; Seo et al., 2010; Steiner et al., 1999; Villarini and Krajewski, 2009; Wilson and Brandes, 1979). Therefore, radar QPE are often combined with rain gauge data to produce more accurate QPE. Rain gauges, however, are also subject to numerous sources of error such as the wind effects, mechanical and/or electronic malfunction, biological contamination as well as systematic biases from wind and turbulence intensity profiles (Essery and Wilcock, 1990; Fankhauser, 1998; Sevruk et al., 1991). In addition, due to the difference in spatiotemporal scale of sampling between rain gauges and radar, the statistical properties of radar precipitation estimates may be significantly different from those of rain gauge measurements (Gires et al., 2014; Li et al., 2013; Westcott et al., 2008). As such, it is necessary to take into account possible biases in the mean and variance in the merging process as well as in evaluation (Seo and Breidenbach, 2002). Rain gauge observations are nevertheless often

considered as truth because they directly measure surface precipitation at points whereas radar precipitation estimates are based on sampling volumes often well above the ground surface.

In an attempt to utilize rain gauge observations in addition to radar data, many linear and nonlinear merging techniques have been reported for multisensor QPE. They may be grouped into linear (Creutin et al., 1988; Delrieu et al., 2014; Goudenhoofdt and Delobbe, 2009; Sinclair and Pegram, 2005; Velasco-Forero et al., 2009) and nonlinear (Azimi-Zonooz et al., 1989; García-Pintado et al., 2009; Hong et al., 2005; Komma et al., 2007; Matsoukas et al., 1999; Seo, 1996) types. Cokriging, for example, is one of the most widely used geostatistical merging techniques (Goudenhoofdt and Delobbe, 2009; Haberlandt, 2007; Krajewski, 1987; Seo et al., 1990; Sideris et al., 2014). Its variants (Seo, 1998a,b) are currently used for radar-gauge analysis in the National Weather Service (NWS) Multisensor Precipitation Estimator (MPE, Seo et al., 2010). Kriging, cokriging and their variants are often considered the best linear unbiased estimators because they are unbiased and minimize error variance in the unconditional sense (Journel and Huijbregts, 1978). In the conditional sense, however, these optimal estimation techniques frequently underestimate large precipitation and overestimate small precipitation. This is because, to minimize error variance unconditionally, the above estimators reduce errors primarily over the median range of precipitation amounts, which occur far more frequently than those at the tail ends of the distribution (Ciach et al., 2000; Habib et al., 2013; Seo and Breidenbach, 2002). Therefore, given some large amount of true rainfall, the conditional mean of its estimates may differ significantly. The difference between the truth and the conditional mean is called conditional mean error or conditional bias (CB) (Ciach et al., 2000). For accurate estimation specifically of large amounts, it is at least as important to reduce CB, in particular Type-II CB. Type-I and -II CBs emerge from Type-I and -II errors, respectively. A Type-I error

92 is associated with a false alarm (e.g. crying wolf without a wolf in sight) whereas a Type-II error
93 is associated with failing to raise an alarm (i.e. failing to see the wolf). Type-I CB can be reduced
94 by scaling up or down (i.e., calibrating) the predicted amounts for the events of interest until CB
95 for the events is reduced (e.g. if the false alarm rate is too high, one may not cry wolf as often).
96 With Type-II CB, however, such calibration is not possible because the analysis system has
97 failed to detect the events at all (Seo et al., 2014). As such, reducing Type-II CB addresses an
98 important gap in multisensor QPE. Toward the above end, conditional bias-penalized kriging
99 (CBPK, Seo, 2012) has been developed for gauge-only analysis (GO) which minimizes Type-II
100 CB (herein denoted as CB for brevity) in addition to unconditional error variance. More recently,
101 extended CB-penalized kriging (ECBPK, Seo et al., 2014) has been developed to address
102 negative estimates in areas of light precipitation and to adjust positive estimates by multiplying a
103 fractional coverage (FC)-dependent scaling factor. They showed that ECBPK significantly
104 improves estimation of heavy-to-extreme precipitation over the variant of ordinary kriging (OK)
105 currently used in the NWS's MPE algorithm for GO. Explicit minimization of CB in multisensor
106 QPE, however, has not been investigated yet.

107 The main objective of this study is to improve multisensor estimation of heavy-to-extreme
108 precipitation via conditional bias-penalized cokriging (CBPCK). Unlike conventional ordinary
109 cokriging (OCK) or its variants which are susceptible to CB, CBPCK explicitly minimizes both
110 unconditional error variance and CB thereby improving performance for estimation of
111 precipitation at tail ends. To evaluate CBPCK, cross validation experiments are designed and
112 carried out over the North Central Texas area using 10 years' worth of hourly data. For
113 comparison, the MPE algorithms for gauge-only and radar-gauge analyses are also run. To assess

performance under different conditions of biasedness in radar QPE, OCK and CBPCK are evaluated with and without bias correcting radar QPE.

2. Data and methodology

In this section, we describe the data used, quality control of the rain gauge data, merging techniques used, parameter estimation, and evaluation metrics.

2.1. Data used

The analysis domain is a 560 x 560 km^2 area in the North Central Texas region (see Fig. 1). The climate of the domain is humid-subtropical with hot summers and relatively mild winters. Mean annual precipitation varies considerably, ranging from less than 500 mm to the west to more than 1200 mm to the east. The rain gauge data used are from the Hydrometeorological Automated Data System (HADS) which is operated by the NWS Office of Hydrologic Development (now the Office of Water Prediction). A total of 199 rain gauges out of 243 within the analysis domain are chosen following a set of quality control steps. The radar data used are from Multi-Radar Multi-Sensor (MRMS) reanalysis (Nelson et al., 2010; Zhang et al., 2015) at the National Centers for Environmental Information (NCEI, formerly the National Climatic Data Center) for which the primary source is the NEXt generation RADar (NEXRAD, Heiss et al., 1990). The MRMS QPE algorithms are largely based on the National Mosaic and multisensor QPE (NMQ) components (Zhang et al., 2011). The MRMS incorporates data from different observing systems to create high-resolution national multisensor QPE for various applications such as flash flood and flood warnings, and water resources management. The MRMS generates multiple products including radar-only, local bias-corrected radar, and gauge-only QPEs. In this work, hourly radar-only QPE from MRMS reanalysis carried out at NCEI was used. The reanalysis period is 10 years, 2002 to 2011. The MRMS products were evaluated over the twelve

River Forecast Center service areas in the contiguous US using rain gauge observations from the Automated Surface Observing System (Wu et al., 2011). The results indicated that the radar-only QPE from MRMS have higher correlation and lower bias compared to those from the Weather Surveillance Radar-1988 Doppler version (WSR-88D) Precipitation Processing Subsystem (Fulton et al., 1998). The radar data used in this work are on a 502 × 502 grid over the analysis domain with a spatial resolution of 0.01° × 0.01°. The upper-left corner of the analysis domain is 35.01 °N and 99.00 °W.

2.2. Data quality control (QC)

Rain gauge observations are subject to various sources of error such as wind, mechanical malfunction, electronic malfunction, and biological contamination (Essery and Wilcock, 1990; Fankhauser, 1998; Sevruk et al., 1991). In this work, the rain gauge data are quality-controlled before being used in multisensor QPE. A cap of 125 mm is applied to hourly rain gauge observations based on the 100-year hourly precipitation in the analysis domain (Frederick et al., 1977; Stevenson and Schumacher, 2014). To quality-control individual rain gauges, the probability of precipitation (PoP) and the conditional (on positive precipitation) coefficient of variation (CV) of hourly gauge precipitation are calculated for each gauge for the entire period of record (Seo and Breidenbach, 2002). The PoP is calculated by the number of positive gauge reports divided by the total number of gauge reports. Based on the regional climatology represented by the general pattern of the statistics, the minimum and maximum thresholds of PoP and conditional CV are applied, respectively. If the PoP of rain gauge is less than 0.02 or the conditional CV of the rain gauge precipitation is larger than 3.2, the gauge is considered suspect and discarded. Each rain gauge observation is then compared with the neighboring gauge observations and, if determined to be outliers (e.g. Fulton et al., 1998), is filtered out.

Gauge observations are also compared with radar data to screen out stuck or malfunctioning rain gauges. Because it is difficult to determine such gauges from hourly data, the rain gauge data are accumulated monthly and visually inspected against monthly accumulated radar QPE. Visual examination of precipitation accumulations at scales smaller than a month is very labor intensive and is not considered in this work. To retain as much data as possible, only those data associated with suspicious months are excluded. Other statistics, such as the unconditional and conditional mean of gauge and radar precipitation, the ratio of the sum of gauge precipitation to the sum of radar precipitation and the indicator and conditional correlation coefficients between gauge and radar precipitation are also examined to aid data quality control (not shown).

2.3. Merging techniques

In this section, we provide a summary description of the two different merging techniques: (1) the variant of OCK used in MPE (Seo et al., 2010) in NWS; and (2) the bivariate version of ECBPK (ECBPK, Seo et al., 2014) or CBPCK.

2.3.1. Ordinary cokriging (OCK)

OCK estimates the precipitation amount at an ungauged location given the neighboring rain gauge observations and the radar QPE. The OCK estimator has the following form:

$$G_k^*(u_0) = \sum_{i=1}^{n_g} \lambda_{gi}\, G_k(u_i) + \sum_{j=1}^{n_r} \lambda_{rj}\, R_k(u_j) \quad (1)$$

$$\sum_{i=1}^{n_g} \lambda_{gi} + \sum_{j=1}^{n_r} \lambda_{rj} = 1 \quad (2)$$

where $G_k^*(u_0)$ denotes the estimated precipitation at the ungauged bin centered at location u_0 in hour k, $G_k(u_i)$ and $R_k(u_j)$ denote the gauge and radar precipitation at location u_i in hour k,

respectively, λ_{gi} and λ_{rj} denotes the weights given to the i-th gauge and the j-th radar data, respectively, n_g and n_r denote the number of gauge and radar data used, respectively. The constraint, Eq. (2), renders the estimate $G_k^*(u_0)$ in Eq. (1) unbiased in the mean sense. The weights given to the nearest gauge and radar data, λ_{gi} and λ_{rj} in Eq. (1), respectively, are obtained by minimizing the error variance of $G_k^*(u_0)$ (see Seo, 1998a,b for details). Note that the choice of the constraint, Eq. (2), assumes that the radar precipitation estimates, $R_k(u_j)$, are unbiased.

The optimal weights, λ_{gi} and λ_{rj}, can be obtained by minimizing the error variance of the estimate, J_{OCK}:

$$J_{OCK} = Var[G_k^*(u_0) - G_k(u_0)] = E[\{G_k^*(u_0) - G_k(u_0)\}^2] = 1 - \sum_{i=1}^{n_g+n_r} \lambda_i \rho_{i0} - \mu \quad (3)$$

where μ denotes the Lagrange multiplier (Journel and Huijbregts, 1978). The optimal weights are a function of the covariance among the gauge observations, that among the radar data and the cross-covariance among the gauge and radar precipitation. The (cross-) covariance is given by (Seo, 1998a,b):

$$\begin{aligned} &Cov\big[G(u_i), R\big(u_j\big)\big] = E[G(u_i) \cdot R(u_i)] - E[G(u_i)] \cdot E[R(u_i)] \\ &= E\big[G(u_i) \cdot R(u_i) | G(u_i) > 0, R\big(u_j\big) > 0\big] \cdot Pr\big[G(u_i) > 0, R\big(u_j\big) > 0\big] \\ &\quad - E[G(u_i) | G(u_i) > 0] \cdot Pr[G(u_i) > 0] \cdot E\big[R\big(u_j\big) \big| R\big(u_j\big) > 0\big] \cdot Pr[R\big(u_j\big) > 0] \end{aligned} \quad (4)$$

In the above, the time index *k* is dropped for notational brevity. Eq. (4) can be rewritten as:

$$\begin{aligned} &Cov\big[G(u_i), R\big(u_j\big)\big] = \sigma_g \sigma_r \big[m_{Ig}\big(1 - m_{Ig}\big)\big]^{1/2} [m_{Ir}(1 - m_{Ir})]^{1/2} \rho_c\big(\big|u_i - u_j\big|\big) \rho_{Ic}\big(\big|u_i - u_j\big|\big) + \\ &m_g m_r [m_{Ig}\big(1 - m_{Ig}\big)]^{1/2} [m_{Ir}(1 - m_{Ir})]^{1/2} \rho_{Ic}\big(\big|u_i - u_j\big|\big) + \sigma_g \sigma_r m_{Ig} m_{Ir} \rho_c\big(\big|u_i - u_j\big|\big) \end{aligned} \quad (5)$$

where σ_g and σ_r denote the standard deviation of gauge and radar precipitation, respectively, m_{Ig} and m_{Ir} denote the mean fractional coverage (FC) of gauge and radar precipitation,

respectively, m_g and m_r denote the unconditional mean of gauge and radar precipitation, respectively, and $\rho_c(|u_i - u_j|)$ and $\rho_{Ic}(|u_i - u_j|)$ denote the conditional and indicator (cross-) correlation at a separation distance of $|u_i - u_j|$, respectively. Under the assumption of homogeneity, the mean FC of precipitation is equivalent to the probability of precipitation (PoP) (Seo and Smith, 1996). As in Seo (1998b), it is assumed in Eq. (5) that σ_g is the same as σ_r, m_{Ig} is the same as m_{Ir}, $\rho_c(|u_i - u_j|)$ is the same as $\rho_{Ic}(|u_i - u_j|)$ and m_g is the same as m_r. These assumptions reduce Eq. (5) to:

$$Cov[G(u_i), R(u_j)] = \sigma_r^2 \cdot [m_{Ir}(1 - m_{Ir})] \cdot \rho_c(|u_i - u_j|) \cdot \rho_{Ic}(|u_i - u_j|) + m_r^2 \cdot [m_{Ir}(1 - m_{Ir})] \cdot \rho_{Ic}(|u_i - u_j|) + \sigma_r^2 \cdot m_{Ir}^2 \cdot \rho_c(|u_i - u_j|) \quad (6)$$

Once the covariance terms are specified, the optimal weights in Eqs. (1) and (2) are obtained by solving the so-called kriging system (Journel and Huijbregts, 1978):

$$\begin{bmatrix} C_{GG} & \cdots & C_{GR} & 1 \\ \vdots & \ddots & \vdots & \vdots \\ C_{RG} & \cdots & C_{RR} & 1 \\ 1 & \cdots & 1 & 0 \end{bmatrix} \begin{bmatrix} \lambda_i \\ \vdots \\ \lambda_{i+j} \\ \mu \end{bmatrix} = \begin{bmatrix} C_{0G} \\ \vdots \\ C_{0R} \\ 1 \end{bmatrix} \quad (7)$$

where C_{GG}, C_{GR} (=C_{RG}^T), and C_{RR} denote the $(n_g) \times (n_g)$, $(n_g) \times (n_r)$, $(n_r) \times (n_r)$ (cross-) covariance matrices whose entries are given by $Cov[G(u_i), G(u_i)]$, $Cov[G(u_i), R(u_j)]$ and $Cov[R(u_j), R(u_j)]$, respectively, and C_{0G} and C_{0R} denote the $(1) \times (n_g)$ and $(1) \times (n_r)$ (cross-) covariance vectors whose entries are given by $Cov[G(u_0), G(u_i)]$ and $Cov[G(u_0), R(u_j)]$, respectively ($i = 1, \ldots, n_g, j = 1, \ldots, n_r$). If our interest is only in the estimate and not in the estimation of variance, OCK may be performed using correlation instead of covariance. Dividing Eq. (6) with the variance of radar precipitation, $Var[R(u)] = \sigma_r^2 \cdot m_{Ir} + m_r^2 \cdot m_{Ir}(1 - m_{Ir})$, results in the correlation between $G(u_i)$ and $R(u_j)$ being:

$$Corr[G(u_i), R(u_j)] = \{CV_r^2 \cdot (1 - m_{Ir}) \cdot \rho_c(|u_i - u_j|) \cdot \rho_{Ic}(|u_i - u_j|) +$$

$$(1 - m_{Ir}) \cdot \rho_{Ic}(|u_i - u_j|) + CV_r^2 \cdot m_{Ir} \cdot \rho_c(|u_i - u_j|)\}/\{CV_r^2 + (1 - m_{Ir})\} \quad (8)$$

where CV_r denotes the coefficient of variation (CV) of radar precipitation.

2.3.2. Conditional bias-penalized cokriging (CBPCK)

Here we describe CBPCK which is the bivariate version of ECBPK (Seo et al., 2014). In CBPCK, the CB penalty term $E[\{E[G^*(u_0)|G(u_0)] - G(u_0)\}^2]$ is added to the objective function where the time index *k* has also been dropped for notational brevity:

$$J_{CBPCK} = E[\{G^*(u_0) - G(u_0)\}^2] + \alpha \bullet E[\{E[G^*(u_0)|G(u_0)] - G(u_0)\}^2] \quad (9)$$

where α denotes the positive weight given to the CB penalty term. The weight, α, can be optimized to improve the balance between reducing error variance and reducing CB. If α is zero, J_{CBPCK} is equivalent to J_{OCK} described in Section 2.3.1. To specify $E[G^*(u_0)|G(u_0)]$ in Eq. (9), the Bayesian optimal estimator (Schweppe, 1973) is used (see Eq. (4) of Seo et al., 2014). The CBPCK system then results from minimizing J_{CBPCK} in Eq. (9) with respect to the weights, $\lambda_j's$:

$$\sum_{j=1}^{n_g+n_r} \lambda_j \left(\rho_{ij} + \alpha \cdot \rho_{i0} \cdot \rho_{j0}\right)\sigma_i \cdot \sigma_j = (1 + \alpha)\rho_{i0} \cdot \sigma_i \cdot \sigma_0 \quad i = 1, \dots, n_g + n_r \quad (10)$$

$$\sum_{i=1}^{n_g} \lambda_{gi} + \sum_{j=1}^{n_r} \lambda_{rj} = 1 \quad (11)$$

where ρ_{ij} denotes the (cross-) correlation between the two variables at u_i and u_j.

As formulated above, CBPCK often produces negative estimates in the areas of light precipitation (see Seo, 2011; Seo et al., 2014). As with OCK, CBPCK is a second-order estimator with no distribution assumptions. As such, if the variable of interest is non-negative, it is necessary to "correct" all negative estimates and reset them to zero. Such thresholding, however, necessarily impacts theoretical unbiasedness of CBPCK negatively. The introduction

of γ removes the biases introduced by the thresholding. Because negative CBPCK estimates are more likely to occur where precipitation occurs only in parts of the local estimation domain, we condition γ on FC. For further details and theoretical justification, the reader is referred to Seo et al. (2015).

$$G^*(u_0)'_{CBPCK} = \begin{cases} 0 & if\ \ G^*(u_0)_{CBPCK} < 0 \\ \gamma \cdot G^*(u_0)_{CBPCK} & otherwise \end{cases} \quad (12)$$

where $G^*(u_0)'_{CBPCK}$ denotes the bias-corrected CBPCK estimate and the scaling coefficient, γ, is empirically estimated as a function of FC of precipitation over the ungauged location by:

$$\gamma = \frac{E[G^*(u_0)_{CBPCK}]}{E[G^*(u_0)_{CBPCK}|G^*(u_0)_{CBPCK}>0]} \quad (13)$$

where $E[G^*(u_0)_{CBPCK}]$ denotes the spatiotemporal mean of CBPCK estimate, $G^*(u_0)$, at location u_0 and $E[G^*(u_0)_{CBPCK}|G^*(u_0)_{CBPCK} > 0]$ denotes the spatiotemporal mean of positive CBPCK estimate, $G^*(u_0)$. The scaling coefficient, γ, is estimated for each subrange of FC of precipitation where FC is calculated by dividing the number of neighboring positive observations by the total number of neighboring observations. If there are no gauge or radar data within the radius of influence, FC is estimated by using the radar or gauge data only, respectively. If there exist both gauge and radar data within the radius of influence, FC is estimated via arithmetic averaging of the two.

While CBPK is superior to OK over the tail ends of the precipitation distribution, it is inferior over the mid-ranges as shown for GO (Seo, 2012). As such, we may choose between CBPCK and OCK based on the more skillful estimation available depending on the magnitude of the true precipitation. In reality, we of course do not know what the true precipitation amount is at the ungauged location. Given that the OCK estimate reflects precipitation information in both

rain gauge and radar data, we consider the OCK estimate at the ungauged location to be the most skillful estimate in this work. Because only the relative position of the ungauged precipitation in the distributional sense, rather than the absolute accuracy, matters in choosing OCK vs. CBPCK, the OCK estimate is transformed into the standard normal deviate, $Z_{OCK,}$ and the weight given to the CB term, α, is specified based on the Z_{OCK} through a simple functional relationship. As a result, in the mid-ranges of the transformed normal distribution, Z_{OCK} is close to zero (i.e. α is very small) and hence the final estimate is closer to the OCK estimate, whereas in the tails Z_{OCK} is large (i.e. α is large) and hence the final estimate is closer to the CBPCK estimate. Due to the different quality in radar-only QPE, two different relationships between α and Z_{OCK} are used for two analysis periods. The relationships used are $\alpha=0.5Z_{OCK}^2$ for the analysis period of 2002 to 2008 and $\alpha=0.286Z_{OCK}^2$ for the analysis period of 2008 to 2011 based on sensitivity analysis.

2.4. Parameter estimation

The merging algorithms used in this work require modeling spatial covariance structures of intermittency and inner variability of precipitation (Seo, 1998a,b). In this work, the correlograms are estimated using the hourly radar QPE under the assumption that the correlogram structures of gauge precipitation are the same as those of radar precipitation (Seo, 1998b). OCK requires specification of the following parameters: the number of nearest neighbors, conditional and indicator correlation models for warm and cool seasons, and CV of point precipitation. Each correlation model requires specification of the model type (exponential, Gaussian or spherical) and correlation scale, both of which are assumed to be common between radar and gauge precipitation, and lag-0+ correlation of radar and gauge precipitation and lag-0 cross correlation between radar and gauge precipitation. The lag-0+ cross correlation is assumed to be the same as the lag-0 cross correlation. CBPCK additionally requires the coefficient C in $\alpha=C\cdot Z_{OCK}^2$. In

286 reality precipitation fields are generally anisotropic. To determine anisotropy, directional
287 experimental correlograms are estimated along the angles of 0°, 26.6°, 45°, 63.4°, 90°, 116.6°,
288 135°, and 153.4° counterclockwise from due east. Each experimental correlogram is then fitted
289 with the exponential, Gaussian, and spherical models with the nugget effect, sill and range as the
290 model parameters (Journel and Huibjbregts, 1978). For both the conditional and indicator
291 correlograms, the exponential model provided the best fit for most cases. As such, we used the
292 exponential model in all analyses. Using directional correlograms, one may visualize 2-
293 dimensional spatial correlation structure by contour-plotting the correlation coefficients. Fig. 2
294 presents the contour plots of the conditional and indicator correlograms for Aug and Nov. The
295 isotropic structure in Aug is associated with convective precipitation in the warm season,
296 whereas the anisotropic structure in Nov is associated with frontal precipitation in the cool
297 season. Because the exponential model provides the best fit for all cases examined and the
298 anisotropic correlation structures are not strong for most months, averages of the parameter
299 values associated with all directional correlation functions were used. Because it is impractical to
300 estimate time-varying covariance structures due to lack of data and large computing
301 requirements, climatological correlograms from the 7-year period of 2002 to 2008 in Table 1
302 were used in this study. The use of climatological (warm vs. cool season) correlation structure, as
303 opposed to flow-dependent structure that varies dynamically, renders the OCK and CBPCK
304 estimates less than optimal (Seo and Smith, 1996; Y. Zhang et al., 2015a, 2015b). The impact of
305 such suboptimal modeling of correlation structure is generally much larger for unconstrained
306 estimators such as simple kriging or simple co-kriging whose weights are not constrained to sum
307 to unity. In practice, time-varying modeling of correlation structure is only feasible for radar
308 precipitation estimates. Note that, even with simplifying assumptions (Seo, 1998), one still has to

estimate time-varying cross correlation coefficients between radar and rain gauge precipitation, a tall order in most areas where rain gauges are sparse. For comparison between OCK and CBPCK, one may expect the impact of the above approximation to be small because the two techniques share the same climatological correlation structure. Additional research is needed, however, to quantify the marginal value of time-varying correlation structure for OCK or CBPCK and to characterize the spatiotemporal structures of nonstationary rainfall fields (see, e.g., Schleiss et al., 2014). The radius of influence for the neighboring observations is specified by the indicator correlation scale. The FC of precipitation within the radius of influence is specified dynamically from rain gauge and radar data at each analysis time by dividing the number of neighboring positive precipitation-reporting observations by the total number of neighboring observations that include zero precipitation. If both data sources are not available within the radius of influence, FC is estimated by using only a single source. The number of neighbors used in the estimation process is 30, as determined from sensitivity analysis. The actual number of rain gauges used, however, may vary from hour to hour because only those rain gauges inside of the radius of influence are used in the estimation process.

2.5. Evaluation metrics

To evaluate the proposed method, cross validation was carried out. For evaluation, different performance metrics and plots, such as scatter and quantile-quantile (QQ) plots, were used. The evaluation metrics used are root mean squared error (RMSE), reduction and percent reduction in RMSE, conditional mean, and multiplicative bias. The RMSE conditioned on the minimum threshold of gauge precipitation is used to measure the conditional performance of the estimators. The RMSE is defined as:

$$\text{RMSE} = \sqrt{\frac{1}{n}\sum_{i=1}^{n}[G^*(u_i) - G(u_i)]^2} \quad (14)$$

where $G^*(u_i)$ denotes the estimated precipitation at location u_i, $G(u_i)$ denotes the rain gauge precipitation at location u_i, and n denotes the total number of observations.

The percent reduction in RMSE by CBPCK over OCK, or $PRiRMSE(CBPCK)$, is defined as:

$$PRiRMSE(CBPCK) = \frac{RMSE(OCK) - RMSE(CBPCK)}{RMSE(OCK)} \times 100 \quad (15)$$

where $RMSE(CBPCK)$ and $RMSE(OCK)$ denote the RMSEs of CBPCK and OCK estimates, respectively.

The multiplicative bias is defined as the ratio of the sum of the estimates to the sum of the verifying observations:

$$\text{Multiplicative Bias} = \frac{\sum_{i=1}^{n} G^*(u_i)}{\sum_{i=1}^{n} G(u_i)} \quad (16)$$

3. Results

This section presents the evaluation results through cross validation and visual examination for the analysis period of 2002 to 2011. All results are based on hourly analysis. Merged fields of hourly precipitation are accumulated to daily to monthly fields as well for visual assessment. Before comparing results using various metrics, we assess the impact of global and monthly bias correction.

3.1. Bias correction

The purpose of this correction is to eliminate or reduce biases in radar QPE due to uncertain Z-R relationship, lack of calibration and temporal changes in the raindrop size distribution (Smith and Krajewski, 1991). The OCK and CBPCK techniques, as formulated in this work, assume that the radar precipitation estimates are unbiased. In reality, however, the radar QPE may be biased due to various error sources. It is hence necessary to assess how the performance of CBPCK may vary depending on the presence of bias in the radar-only QPE. In this work, mean field bias correction (Anagnostou et al., 1998; Seo et al., 1999; Smith and Krajewski, 1991; Y. Zhang et al., 2011) is applied separately by multiplying the bias correction factor to radar QPE before OCK or CBPCK is performed. The bias correction factor β defined as:

$$\beta = \frac{\sum_i^n [G_k(u_i) | G_k(u_i)>0,\, R_k(u_i)>0]}{\sum_i^n [R_k(u_i) | G_k(u_i)>0,\, R_k(u_i)>0]} \quad (17)$$

The global bias correction factor is a single number calculated using all positive-positive pairs of collocated hourly gauge and radar rainfall data at rain gauge locations at every hour k for the entire period of analysis. Because of the different quality of radar data, two global bias correction factors are estimated for two analysis periods of 2002 to 2008 and 2008 to 2011. In the global sense, the radar data tend to underestimate gauge precipitation for the period of 2002 to 2007 whereas they tend to overestimate for the period of 2009 to 2011. The radar data for 2008 show no significant bias and are included in both analysis periods. The global bias correction factors estimated for two periods of 2002 to 2008 and 2008 to 2011 are 1.05 (radar underestimate by 5%) and 0.90 (radar overestimate by 10%), respectively. For the entire period of 2002 to 2011, the global bias correction factor is close to unity. The monthly bias correction factors are also calculated for two periods (see Fig. 3). The figure shows that the monthly bias correction factors are generally larger for 2002 to 2008 than for 2008 to 2011, and that the radar QPE generally

over- and underestimate gauge precipitation during the warm and cool seasons, respectively. Note that, the global and monthly bias correction factors do not account for spatial variability of bias since a single value is used for the entire domain.

3.2. Cross validation

To evaluate the proposed technique, leave-one-gauge-out cross validation is performed using hourly radar QPE and rain gauge observations. The cokriging parameters are estimated using all available data in a dependent validation mode. For the cokriging parameters, we could have carried out true validation or leave-one-year-out cross validation in which the parameter estimation and validation periods are separated. Our choice for dependent validation in this work is based on the observation that, at multi-annual scale, the cokriging parameters do not vary significantly. The above observation is not surprising in that the parameters are seasonal and reflect a rather large area. The leave-one-gauge-out cross validation process comprise the following steps: 1) withhold hourly rain gauge observations one at a time and estimate precipitation at the withheld gauge location using all available data; 2) compare the estimated amount with the revealed rain gauge observation; 3) repeat the above steps for all rain gauge locations in the entire cross-validation period. Cross validation is performed for OCK, CBPCK, and GO. Fig. 4 shows the percent reduction in RMSE by OCK over RO and by CBPCK over RO conditional on the verifying gauge precipitation greater than that shown on the x-axis following monthly and global bias correction. For the analysis period of 2002 to 2008, bias correction shows little impact. In general, positive reduction in RMSE by CBPCK and OCK over RO can be seen regardless of the threshold for verifying gauge precipitation amount. CBPCK is superior to OCK over thresholds greater than 30mm but shows limited performance over thresholds less than 30 mm. For 2008 to 2011, the monthly and global bias correction before merging provide

noticeable improvement in OCK whereas the positive impact is only marginal for CBPCK. For this period, OCK is inferior to RO except at the tail ends whereas CBPCK is superior or comparable to RO at all thresholds. For large precipitation amounts, significant reduction of up to 20% in RMSE by CBPCK over RO is seen. Overall, compared to global bias correction, monthly bias correction slightly improves the relative performance by OCK over RO. The relative performance by CBPCK over RO, on the other hand, does not change much between the two bias correction methods. Given that the impact of bias correction is only marginal, below we present the results without bias correction.

Fig. 5 shows the reduction in RMSE by CBPCK (green) and OCK (red) over RO conditional on the verifying gauge precipitation greater than that shown on the x-axis. The reduction in RMSE is conditioned also on FC. The conditions, FC > 0 (solid line) and FC > 0.9 (dotted line), indicate that the fractional coverage of precipitation over the ungauged location is greater than 0 and 0.9, respectively. A very high FC means that it is most likely to be precipitating over the ungauged location. When FC > 0.9 and hourly gauge precipitation is greater than 60 mm, the reduction in RMSE by CBPCK over RO is about 12 mm. The results show that, the larger the precipitation amount and FC are, the larger the reduction in RMSE by both CBPCK and OCK over RO is. When FC is high, the margin of improvement by CBPCK is greater than that by OCK. When FC is high, both CBPCK and OCK have smaller RMSE than RO regardless of the minimum gauge precipitation. Note also that CBPCK is superior to OCK regardless of FC. Fig. 6 shows the multiplicative bias of the OCK and CBPCK estimates relative to the verifying truth conditional on the verifying gauge precipitation exceeding the threshold shown on the x-axis for FC > 0 and FC > 0.9. Although large biases are observed in both the OCK and CBPCK estimate, significant reduction in bias is seen when FC is large (i.e., FC > 0.9). The margin of reduction in

418 multiplicative bias by CBPCK over OCK (Fig. 6) also increases as the thresholding gauge
419 precipitation increases. The rather large multiplicative biases seen in the figure reinforce the need
420 for improving estimation of heavy-to-extreme precipitation at point to small spatial scales. For
421 large catchments, such large biases are not likely to exist in mean areal precipitation (MAP)
422 estimates because, in any given hour, only a relatively small fraction of the catchment is likely to
423 be receiving heavy-to-extreme precipitation.

424 Fig. **7** shows the scatter and QQ (in red) plots of the GO, RO, OCK and CBPCK estimates
425 vs. the verifying hourly gauge precipitation only for those data points for which the FC is greater
426 than 0.9. Note that GO (upper-left) and OCK (lower-left) tend to significantly underestimate
427 large precipitation amounts (> 50 mm). RO is reasonably conditionally unbiased in the global
428 sense but generally has a larger scatter compared to OCK and CBPCK. The generally positive
429 impact of CBPCK may be seen particularly for estimation of large precipitation. For small
430 precipitation amounts, however, the limitation of CBPCK may also be seen. The isolated cases
431 of significant overestimation of smaller amounts by CBPCK compared to RO is due to
432 overestimation in the standard normal space by OCK as explained below. It is recalled that the
433 weight, α, for the CB term in CBPCK is specified by the standard normal transform of the OCK
434 estimate. If OCK incorrectly overestimates small amounts, its estimates are associated with large
435 standard normal deviates resulting in large values of α and hence assigning CBPCK estimate
436 rather than OCK estimates. Because of the large analysis domain and multi-year analysis period,
437 the scatter plots include a large number of large amounts of hourly precipitation. As such, the
438 plots illustrate very well the large variability of precipitation in the study area and the challenges
439 for accurate QPE. Lack of representativeness of point gauge precipitation for areal precipitation
440 is an issue due to the often convective nature of the storms in the study area and is a contributing

441 factor to the scatter. The representativeness error, however, does not significantly impact second-
442 order error statistics such as root mean square error (Seo and Breidenbach, 2002).

443 While the global analysis over the long analysis periods represented in Fig. ***7*** is useful for
444 assessment of long-term performance, the relative performance among GO, RO, OCK and
445 CBPCK may depend greatly on specific rainfall events that produce very large to extreme
446 amounts of precipitation. To assess performance within specific time periods of heavy-to-
447 extreme precipitation, the scatter plots of hourly estimates were visually examined for a number
448 of months that produced large amounts of precipitation. Fig. 8 shows an example of the scatter
449 and QQ plots of the hourly estimates for Apr 2008. Note that CBPCK significantly improves
450 over both RO and OCK particularly for estimation of large precipitation amounts. Fig. 9 shows
451 the percent reduction in RMSE as a function of the minimum FC of precipitation over the
452 ungauged location by CBPCK over OCK for hourly gauge precipitation greater than the amount
453 shown on the x-axis. The figure shows that CBPCK is superior to OCK for precipitation amounts
454 greater than 30 mm regardless of FC. For FC > 0.5, the reduction is positive when gauge
455 precipitation exceeds approximately 15 mm and, for verifying precipitation exceeding 40 mm,
456 the reduction is about 8%. If the threshold gauge precipitation is less than 10 mm, however,
457 CBPCK is inferior to OCK regardless of FC. The negative reduction in light precipitation arises
458 from the fact that OCK minimizes unconditional error variance and hence does better than
459 CBPCK for precipitation amounts around the median. Note that, the larger the precipitation
460 amount is, the larger the percent reduction in RMSE by CBPCK is over OCK, and that, the larger
461 the FC is, the larger the percent reduction in RMSE is. Fig. 10 shows the conditional mean of the
462 gauge (denoted as truth), RO, OCK and CBPCK estimates for hourly point precipitation amounts
463 greater than that shown on the x-axis for FC > 0.9. The figure indicates that CBPCK reduces

conditional mean bias over OCK for all ranges and over RO for precipitation amounts exceeding 50 mm. The margin of improvement by CBPCK over OCK increases as the threshold of verifying precipitation increases.

3.3. Precipitation maps

The hourly multisensor analyses are accumulated up to a month for visual assessment of the performance of each technique. Fig. 11 shows an example of the hourly analysis fields from GO, RO, OCK and CBPCK valid at 9 pm on Mar 18, 2008. The GO field is generated using ECBPK (Seo et al., 2014). The complementary nature of the multisensor analyses is readily seen. Note that, compared to the OCK analysis, the CBPCK analysis shows increased precipitation in the convective cores. Fig. 12 shows an example of daily accumulation fields valid for Mar 18 obtained by aggregating the hourly results. Similar observations to the hourly example above may be made. Fig. 13 shows an example of monthly accumulation fields valid for Mar 2008 obtained by aggregating the hourly results. While it is not possible to verify the absolute accuracy of the analyses due to lack of ground truth, the above figures suggest that CBPCK is able to capture the variability better than OCK. Fig. 14 shows the differences in monthly precipitation maps shown in Fig. 13. RO tends to underestimate the large precipitation amounts seen in GO. The difference between the monthly OCK and CBPCK fields ranges from -25 to 70 mm. Note that CBPCK significantly increases estimates in areas of heavy precipitation while decreasing estimates over areas of light precipitation.

4. Conclusions and future research recommendations

A new multisensor QPE technique for gauge-radar analysis, conditional bias-penalized cokriging (CBPCK), is developed to improve estimation of heavy-to-extreme precipitation. Unlike conventional ordinary cokriging (OCK) or its variants which are susceptible to

conditional bias (CB), CBPCK explicitly minimizes both unconditional error variance and Type-II CB thereby improving performance for estimation of precipitation at tail ends. For evaluation, multi-year leave-one-gauge-out cross validation was carried out for comparative evaluation of CBPCK with the variant of ordinary cokriging (OCK, Seo, 1998 a,b) currently used in the NWS's multisensor precipitation estimator (MPE). The analysis domain is a 560 x 560 km^2 area in the North Central Texas region. The main findings and conclusions are as follows**.** CBPCK improves over OCK for estimation of hourly precipitation exceeding 30 mm. The margin of improvement depends most significantly on fractional coverage (FC) of precipitation at the ungauged location. If FC is 50% or higher, CBPCK reduces RMSE over OCK by approximately 8% for hourly precipitation greater than 40 mm. If FC is 90% or higher (i.e. it is very likely to be precipitating at the ungauged location), the margin of improvement is approximately 15% for hourly precipitation greater than 70 mm. Bias correction of radar-only QPE before merging tends to improve the performance of both OCK and CBPCK. The improvement is noticeable for OCK but marginal at best for CBPCK. Only CBPCK, however, is able to outperform bias-corrected radar-only (RO) consistently. Compared to global bias correction, monthly bias correction is marginally more effective. It is seen that the radar-only QPE from MRMS reanalysis is globally biased high by about 10%, and over- and underestimates gauge precipitation in the warm and cool seasons, respectively. For the data sets used in this work, CBPCK is seen to be capable of improving estimation of heavy-to-extreme precipitation with or without bias correction of RO. Quality control of rain gauge observations remains a large challenge. For objective evaluation, there exists a clear need for high-quality hourly rain gauge data. Visual examination of the analysis results at hourly, daily and monthly scales of accumulation indicates that, compared to OCK, CBPCK increases and decreases the estimated amounts in areas of heavy and light

precipitation, respectively. Because the quality of the weighting factor, α, is only as good as that of the OCK estimates, there are occasions when CBPCK significantly overestimates light precipitation due to mis-prognostication of the magnitude of precipitation at the ungauged location. For more skillful determination of α, it is necessary to incorporate additional sources of precipitation information, such as satellite QPE, lightning observations and numerical weather prediction (NWP) output.

Acknowledgements

This material is based upon work supported by the National Science Foundation under Grant No. CyberSEES-1442735. This support is gratefully acknowledged.

Acronyms

AP: Anomalous propagation

CB: Conditional bias

CBPCK: Conditional bias-penalized co-kriging

CBPK: Conditional bias-penalized kriging

CV: Coefficient of variation

ECBPK: Extended condition bias-penalized kriging

FC: Fractional coverage

GO: Gauge-only analysis

HADS: Hydrometeorological Automated Data System

MRMS: Multi-Radar Multi-Sensor

MPE: Multisensor Precipitation Estimator

NEXRAD: Next Generation Radar

NMQ: National Mosaic and multisensor QPE

NWP: Numerical Weather Prediction

NWS: National Weather Service

OCK: Ordinary co-kriging

OK: Ordinary kriging

PoP: Probability of precipitation

QC: Quality control

QPE: Quantitative precipitation estimation

RMSE: Root mean square error

RO: Radar-only analysis

VPR: Vertical profile of reflectivity

WSR-88D: Weather Surveillance Radar-1988 Doppler version

References

Anagnostou, E.N., Krajewski, W.F., Seo, D.-J., Johnson, E.R., 1998. Mean-Field Rainfall Bias Studies for WSR-88D. J. Hydrol. Eng. 3, 149–159. doi:10.1061/(ASCE)1084-0699(1998)3:3(149)

Austin, P.M., 1987. Relation between Measured Radar Reflectivity and Surface Rainfall. Mon. Weather Rev. 115, 1053–1070. doi:10.1175/1520-0493(1987)115<1053:RBMRRA>2.0.CO;2

Azimi-Zonooz, A., Krajewski, W.F., Bowles, D.S., Seo, D.J., 1989. Spatial rainfall estimation by linear and non-linear co-kriging of radar-rainfall and raingage data. Stoch. Hydrol. Hydraul. 3, 51–67. doi:10.1007/BF01543427

555 Chandrasekar, V., Keränen, R., Lim, S., Moisseev, D., 2013. Recent advances in classification of
556 observations from dual polarization weather radars. Atmospheric Res., ADVANCES IN
557 PRECIPITATION SCIENCE 119, 97–111. doi:10.1016/j.atmosres.2011.08.014
558 Chen, H., Chandrasekar, V., 2015. The quantitative precipitation estimation system for Dallas–
559 Fort Worth (DFW) urban remote sensing network. J. Hydrol., Hydrologic Applications of
560 Weather Radar 531, Part 2, 259–271. doi:10.1016/j.jhydrol.2015.05.040
561 Ciach, G.J., Morrissey, M.L., Krajewski, W.F., 2000. Conditional Bias in Radar Rainfall
562 Estimation. J. Appl. Meteorol. 39, 1941–1946. doi:10.1175/1520-
563 0450(2000)039<1941:CBIRRE>2.0.CO;2
564 Creutin, J.D., Delrieu, G., Lebel, T., 1988. Rain Measurement by Raingage-Radar Combination:
565 A Geostatistical Approach. J. Atmospheric Ocean. Technol. 5, 102–115.
566 doi:10.1175/1520-0426(1988)005<0102:RMBRRC>2.0.CO;2
567 Delrieu, G., Wijbrans, A., Boudevillain, B., Faure, D., Bonnifait, L., Kirstetter, P.-E., 2014.
568 Geostatistical radar–raingauge merging: A novel method for the quantification of rain
569 estimation accuracy. Adv. Water Resour. 71, 110–124.
570 doi:10.1016/j.advwatres.2014.06.005
571 Essery, C.I., Wilcock, D.N., 1990. Checks on the measurement of potential evapotranspiration
572 using water balance data and independent measures of groundwater recharge. J. Hydrol.
573 120, 51–64. doi:10.1016/0022-1694(90)90141-J
574 Fang, M., Doviak, R.J., Melnikov, V., 2004. Spectrum Width Measured by WSR-88D: Error
575 Sources and Statistics of Various Weather Phenomena. J. Atmospheric Ocean. Technol.
576 21, 888–904. doi:10.1175/1520-0426(2004)021<0888:SWMBWE>2.0.CO;2

577 Fankhauser, R., 1998. Influence of systematic errors from tipping bucket rain gauges on recorded
578 rainfall data. Water Sci. Technol., Use of Historical Rainfall Series for Hydrological
579 ModellingSelected Proceedings of the Third International Workshop on Rainfall in Urban
580 Areas 37, 121–129. doi:10.1016/S0273-1223(98)00324-2
581 Frederick, R.H., Myers, V.A., Auciello, E.P., 1977. Five to 60 Minute Precipitation Frequency
582 Atlas of the Western United States. NOAA Tech Memo NWS HYDRO-35.
583 Fulton, R.A., Breidenbach, J.P., Seo, D.-J., Miller, D.A., O'Bannon, T., 1998. The WSR-88D
584 Rainfall Algorithm. Weather Forecast. 13, 377–395. doi:10.1175/1520-
585 0434(1998)013<0377:TWRA>2.0.CO;2
586 García-Pintado, J., Barberá, G.G., Erena, M., Castillo, V.M., 2009. Rainfall estimation by rain
587 gauge-radar combination: A concurrent multiplicative-additive approach. Water Resour.
588 Res. 45, W01415. doi:10.1029/2008WR007011
589 Gires, A., Tchiguirinskaia, I., Schertzer, D., Schellart, A., Berne, A., Lovejoy, S., 2014.
590 Influence of small scale rainfall variability on standard comparison tools between radar
591 and rain gauge data. Atmospheric Res. 138, 125–138.
592 doi:10.1016/j.atmosres.2013.11.008
593 Goudenhoofdt, E., Delobbe, L., 2009. Evaluation of radar-gauge merging methods for
594 quantitative precipitation estimates. Hydrol Earth Syst Sci 13, 195–203.
595 doi:10.5194/hess-13-195-2009
596 Gourley, J.J., Jorgensen, D.P., Matrosov, S.Y., Flamig, Z.L., 2009. Evaluation of Incremental
597 Improvements to Quantitative Precipitation Estimates in Complex Terrain. J.
598 Hydrometeorol. 10, 1507–1520. doi:10.1175/2009JHM1125.1

599 Haberlandt, U., 2007. Geostatistical interpolation of hourly precipitation from rain gauges and
600 radar for a large-scale extreme rainfall event. J. Hydrol. 332, 144–157.
601 doi:10.1016/j.jhydrol.2006.06.028
602 Habib, E., Qin, L., Seo, D.-J., Ciach, G.J., Nelson, B.R., 2013. Independent Assessment of
603 Incremental Complexity in NWS Multisensor Precipitation Estimator Algorithms. J.
604 Hydrol. Eng. 18, 143–155. doi:10.1061/(ASCE)HE.1943-5584.0000638
605 Heiss, W.H., McGrew, D.L., Sirmans, D., 1990. NEXRAD-Next generation weather radar
606 (WSR-88D). Microw. J. 33, 79.
607 Hong, Y., Hsu, K., Sorooshian, S., Gao, X., 2005. Self-organizing nonlinear output (SONO): A
608 neural network suitable for cloud patch–based rainfall estimation at small scales. Water
609 Resour. Res. 41, W03008. doi:10.1029/2004WR003142
610 Journel, A.G., Huijbregts, C.J., 1978. Mining Geostatistics. Academic Press.
611 Kitzmiller, D., Van Cooten, S., Ding, F., Howard, K., Langston, C., Zhang, J., Moser, H., Zhang,
612 Y., Gourley, J.J., Kim, D., Riley, D., 2011. Evolving Multisensor Precipitation
613 Estimation Methods: Their Impacts on Flow Prediction Using a Distributed Hydrologic
614 Model. J. Hydrometeorol. 12, 1414–1431. doi:10.1175/JHM-D-10-05038.1
615 Komma, J., Reszler, C., Blöschl, G., Haiden, T., 2007. Ensemble prediction of floods ?
616 catchment non-linearity and forecast probabilities. Nat. Hazards Earth Syst. Sci. 7, 431–
617 444.
618 Krajewski, W.F., 1987. Cokriging radar-rainfall and rain gage data. J. Geophys. Res.
619 Atmospheres 92, 9571–9580. doi:10.1029/JD092iD08p09571

620 Li, Z., Yang, D., Hong, Y., 2013. Multi-scale evaluation of high-resolution multi-sensor blended
621 global precipitation products over the Yangtze River. J. Hydrol. 500, 157–169.
622 doi:10.1016/j.jhydrol.2013.07.023
623 Marshall, J.S., Hitschfeld, W., Gunn, K.L.S., 1955. Advances in Radar Weather, in: Landsberg,
624 H.E. (Ed.), Advances in Geophysics. Elsevier, pp. 1–56.
625 Matsoukas, C., Islam, S., Kothari, R., 1999. Fusion of radar and rain gage measurements for an
626 accurate estimation of rainfall. J. Geophys. Res. Atmospheres 104, 31437–31450.
627 doi:10.1029/1999JD900487
628 Nelson, B.R., Prat, O.P., Seo, D.-J., Habib, E., 2015. Assessment and Implications of NCEP
629 Stage IV Quantitative Precipitation Estimates for Product Intercomparisons. Weather
630 Forecast. doi:10.1175/WAF-D-14-00112.1
631 Nelson, B.R., Seo, D.-J., Kim, D., 2010. Multisensor Precipitation Reanalysis. J. Hydrometeorol.
632 11, 666–682. doi:10.1175/2010JHM1210.1
633 Schleiss, M., Chamoun, S., Berne, A., 2014. Stochastic simulation of intermittent rainfall using
634 the concept of "dry drift." Water Resour. Res. 50, 2329–2349.
635 doi:10.1002/2013WR014641
636 Schweppe, F.C., 1973. Uncertain dynamic systems. Prentice-Hall.
637 Seo, D., Siddique, R., Ahnert, P., 2014. Objective Reduction of Rain Gauge Network via
638 Geostatistical Analysis of Uncertainty in Radar-Gauge Precipitation Estimation. J.
639 Hydrol. Eng. 20, 4014050. doi:10.1061/(ASCE)HE.1943-5584.0000969
640 Seo, D.-J., 2012. Conditional bias-penalized kriging (CBPK). Stoch. Environ. Res. Risk Assess.
641 27, 43–58. doi:10.1007/s00477-012-0567-z

642 Seo, D.-J., 1998a. Real-time estimation of rainfall fields using radar rainfall and rain gage data. J.
643 Hydrol. 208, 37–52. doi:10.1016/S0022-1694(98)00141-3
644 Seo, D.-J., 1998b. Real-time estimation of rainfall fields using rain gage data under fractional
645 coverage conditions. J. Hydrol. 208, 25–36. doi:10.1016/S0022-1694(98)00140-1
646 Seo, D.-J., 1996. Nonlinear estimation of spatial distribution of rainfall — An indicator cokriging
647 approach. Stoch. Hydrol. Hydraul. 10, 127–150. doi:10.1007/BF01581763
648 Seo, D.-J., Breidenbach, J.P., 2002. Real-time correction of spatially nonuniform bias in radar
649 rainfall data using rain gauge measurements. J. Hydrometeorol. 3, 93–111.
650 doi:10.1175/1525-7541(2002)003<0093:RTCOSN>2.0.CO;2
651 Seo, D.-J., Breidenbach, J.P., Johnson, E.R., 1999. Real-time estimation of mean field bias in
652 radar rainfall data. J. Hydrol. 223, 131–147. doi:10.1016/S0022-1694(99)00106-7
653 Seo, D.-J., Habib, E., Andrieu, H., Morin, E., 2015. Hydrologic applications of weather radar. J.
654 Hydrol., Hydrologic Applications of Weather Radar 531, Part 2, 231–233.
655 doi:10.1016/j.jhydrol.2015.11.010
656 Seo, D.-J., Krajewski, W.F., Bowles, D.S., 1990. Stochastic interpolation of rainfall data from
657 rain gages and radar using cokriging: 1. Design of experiments. Water Resour. Res. 26,
658 469–477. doi:10.1029/WR026i003p00469
659 Seo, D.-J., Seed, A., Delrieu, G., 2010. Radar and Multisensor Rainfall Estimation for
660 Hydrologic Applications, in: Wiley: Rainfall: State of the Science, Volume 191, F.Y.
661 Testik and M. Gebremichael, Editors.
662 Seo, D.-J., Siddique, R., Zhang, Y., Kim, D., 2014. Improving real-time estimation of heavy-to-
663 extreme precipitation using rain gauge data via conditional bias-penalized optimal
664 estimation. J. Hydrol. 519, Part B, 1824–1835. doi:10.1016/j.jhydrol.2014.09.055

665 Seo, D.-J., Smith, J.A., 1996. Characterization of the Climatological Variability of Mean Areal
666 Rainfall Through Fractional Coverage. Water Resour. Res. 32, 2087–2095.
667 doi:10.1029/96WR00486
668 Sevruk, B., Hertig, J.-A., Spiess, R., 1991. The effect of a precipitation gauge orifice rim on the
669 wind field deformation as investigated in a wind tunnel. Atmospheric Environ. Part Gen.
670 Top. 25, 1173–1179. doi:10.1016/0960-1686(91)90228-Y
671 Sideris, I.V., Gabella, M., Erdin, R., Germann, U., 2014. Real-time radar–rain-gauge merging
672 using spatio-temporal co-kriging with external drift in the alpine terrain of Switzerland.
673 Q. J. R. Meteorol. Soc. 140, 1097–1111. doi:10.1002/qj.2188
674 Sinclair, S., Pegram, G., 2005. Combining radar and rain gauge rainfall estimates using
675 conditional merging. Atmospheric Sci. Lett. 6, 19–22. doi:10.1002/asl.85
676 Smith, J.A., Krajewski, W.F., 1991. Estimation of the Mean Field Bias of Radar Rainfall
677 Estimates. J. Appl. Meteorol. 30, 397–412. doi:10.1175/1520-
678 0450(1991)030<0397:EOTMFB>2.0.CO;2
679 Smith, J.A., Seo, D.J., Baeck, M.L., Hudlow, M.D., 1996. An Intercomparison Study of
680 NEXRAD Precipitation Estimates. Water Resour. Res. 32, 2035–2045.
681 doi:10.1029/96WR00270
682 Steiner, M., Smith, J.A., Burges, S.J., Alonso, C.V., Darden, R.W., 1999. Effect of bias
683 adjustment and rain gauge data quality control on radar rainfall estimation. Water Resour.
684 Res. 35, 2487–2503.
685 Stevenson, S.N., Schumacher, R.S., 2014. A 10-Year Survey of Extreme Rainfall Events in the
686 Central and Eastern United States Using Gridded Multisensor Precipitation Analyses.
687 Mon. Weather Rev. 142, 3147–3162. doi:10.1175/MWR-D-13-00345.1

688 Vasiloff, S.V., Howard, K.W., Rabin, R.M., Brooks, H.E., Seo, D.-J., Zhang, J., Kitzmiller,
689 D.H., Mullusky, M.G., Krajewski, W.F., Brandes, E.A., Brown, B.G., Berkowitz, D.S.,
690 McGinley, J.A., Kuligowski, R.J., 2007. Improving QPE and Very Short Term QPF: An
691 Initiative for a Community-Wide Integrated Approach. Bull. Am. Meteorol. Soc. 88,
692 1899–1911. doi:10.1175/BAMS-88-12-1899
693 Velasco-Forero, C.A., Sempere-Torres, D., Cassiraga, E.F., Jaime Gómez-Hernández, J., 2009.
694 A non-parametric automatic blending methodology to estimate rainfall fields from rain
695 gauge and radar data. Adv. Water Resour., Weather Radar and Hydrology 32, 986–1002.
696 doi:10.1016/j.advwatres.2008.10.004
697 Villarini, G., Krajewski, W.F., 2009. Review of the Different Sources of Uncertainty in Single
698 Polarization Radar-Based Estimates of Rainfall. Surv. Geophys. 31, 107–129.
699 doi:10.1007/s10712-009-9079-x
700 Westcott, N.E., Knapp, H.V., Hilberg, S.D., 2008. Comparison of gage and multi-sensor
701 precipitation estimates over a range of spatial and temporal scales in the Midwestern
702 United States. J. Hydrol. 351, 1–12. doi:10.1016/j.jhydrol.2007.10.057
703 Westrick, K.J., Mass, C.F., Colle, B.A., 1999. The Limitations of the WSR-88D Radar Network
704 for Quantitative Precipitation Measurement over the Coastal Western United States. Bull.
705 Am. Meteorol. Soc. 80, 2289–2298. doi:10.1175/1520-
706 0477(1999)080<2289:TLOTWR>2.0.CO;2
707 Wilson, J.W., Brandes, E.A., 1979. Radar Measurement of Rainfall—A Summary. Bull. Am.
708 Meteorol. Soc. 60, 1048–1058. doi:10.1175/1520-
709 0477(1979)060<1048:RMORS>2.0.CO;2

Yamaguchi, K., Kimpara, C., Nakakita, E., 2012. Developing Space-Time Structure of Raindrop Size Distribution and Qpe Method from New Dsd Retrieving Method Using X-Band Polarimetric Radar. J. Jpn. Soc. Civ. Eng. Ser B1 Hydraul. Eng. 68, I_367-I_372. doi:10.2208/jscejhe.68.I_367

Young, C.B., Bradley, A.A., Krajewski, W.F., Kruger, A., Morrissey, M.L., 2000. Evaluating NEXRAD Multisensor Precipitation Estimates for Operational Hydrologic Forecasting. J. Hydrometeorol. 1, 241–254. doi:10.1175/1525-7541(2000)001<0241:ENMPEF>2.0.CO;2

Zhang, J., Howard, K., Langston, C., Kaney, B., Qi, Y., Tang, L., Grams, H., Wang, Y., Cocks, S., Martinaitis, S., Arthur, A., Cooper, K., Brogden, J., Kitzmiller, D., 2015. Multi-Radar Multi-Sensor (MRMS) Quantitative Precipitation Estimation: Initial Operating Capabilities. Bull. Am. Meteorol. Soc. doi:10.1175/BAMS-D-14-00174.1

Zhang, J., Howard, K., Langston, C., Vasiloff, S., Kaney, B., Arthur, A., Van Cooten, S., Kelleher, K., Kitzmiller, D., Ding, F., Seo, D.-J., Wells, E., Dempsey, C., 2011. National Mosaic and Multi-Sensor QPE (NMQ) System: Description, Results, and Future Plans. Bull. Am. Meteorol. Soc. 92, 1321–1338. doi:10.1175/2011BAMS-D-11-00047.1

Zhang, J., Qi, Y., Kingsmill, D., Howard, K., 2012. Radar-Based Quantitative Precipitation Estimation for the Cool Season in Complex Terrain: Case Studies from the NOAA Hydrometeorology Testbed. J. Hydrometeorol. 13, 1836–1854. doi:10.1175/JHM-D-11-0145.1

Zhang, Y., Reed, S., Gourley, J.J., Cosgrove, B., Kitzmiller, D., Seo, D.-J., Cifelli, R., 2015a. The Impacts of Climatological Adjustment of Quantitative Precipitation Estimates on the

Accuracy of Flash Flood Detection. J. Hydrol. in press. doi:10.1016/j.jhydrol.2015.12.017

Zhang, Y., Reed, S., Kitzmiller, D., 2011. Effects of Retrospective Gauge-Based Readjustment of Multisensor Precipitation Estimates on Hydrologic Simulations. J. Hydrometeorol. 12, 429–443. doi:10.1175/2010JHM1200.1

Zhang, Y., Seo, D.-J., Habib, E., McCollum, J., 2015b. Differences in scale-dependent, climatological variation of mean areal precipitation based on satellite and radar-gauge observations. J. Hydrol. 522, 35–48. doi:10.1016/j.jhydrol.2014.11.077

List of figure captions

Fig. 1. Analysis domain (560 x 560 km^2).

Fig. 2. Contour plots of conditional and indicator correlograms for Aug (upper) and Nov (lower).

Fig. 3. Monthly bias correction factor for radar-only QPE.

Fig. 4. Percent reduction in RMSE by OCK and CBPCK over RO without bias correction and with global and monthly bias correction.

Fig. 5. Reduction in RMSE by CBPCK and OCK over RO (2002-2008).

Fig. 6. Multiplicative bias (y-axis) of the precipitation estimate conditional on verifying amount exceeding the threshold (x-axis) for FC > 0 (solid line) and for FC > 0.9 (dashed line) (2002-2008).

Fig. 7. Scatter and QQ plots of the truth vs. the hourly GO, RO, OCK and CBPCK estimates when FC exceeds 0.9 (2002-2008).

Fig. 8. Scatter and QQ plots of the truth vs. the hourly estimates for Apr 2008.

Fig. 9. Percent reduction in RMSE as a function of the minimum FC over the ungauged location by CBPCK over OCK (2002-2008).

Fig. 10. Conditional mean of the gauge (identified as "TRUTH"), RO, OCK and CBPCK estimates for FC > 0.9 (2002-2008).

Fig. 11. Example fields of hourly precipitation from GO (upper-left), RO (upper-right), OCK (lower-left) and CBPCK (lower-right) valid at 9 pm Mar 18, 2008.

Fig. 12. Example fields of daily precipitation from GO (upper-left), RO (upper-right), OCK (lower-left) and CBPCK (lower-right) for Mar 18, 2008.

Fig. 13. Example fields of monthly precipitation from GO (upper-left), RO (upper-right), OCK (lower-left) and CBPCK (lower-right) for Mar 2008.

Fig. 14. Differences in monthly precipitation maps for Mar 2008 between the two estimation techniques shown in the figure title among GO, RO, OCK and CBPCK.

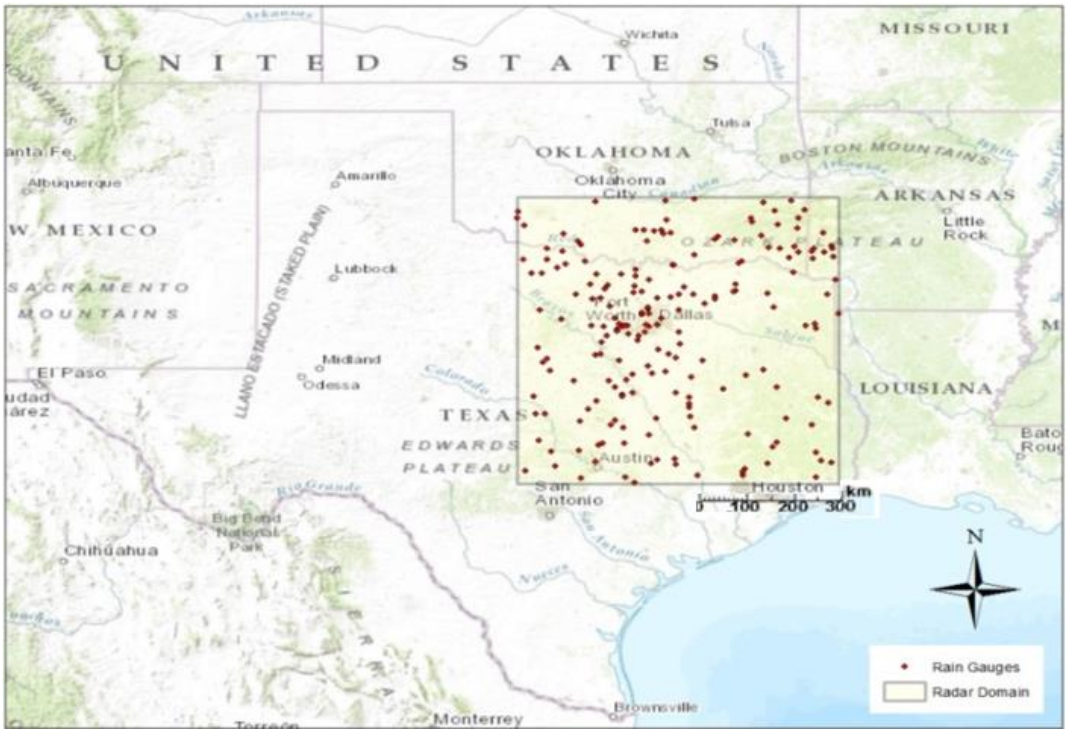

Fig. 1. Analysis domain (560 x 560 km^2).

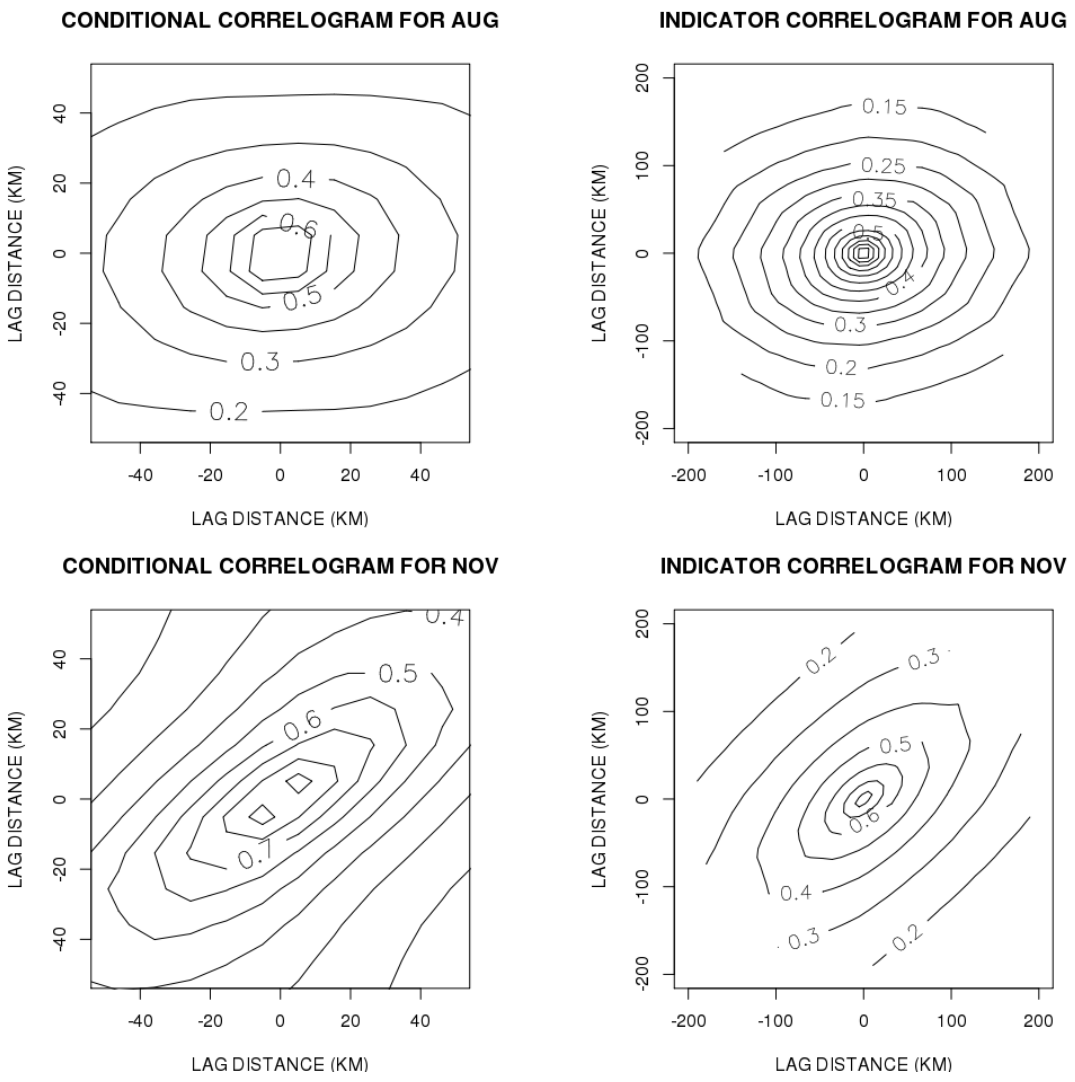

Fig. 2. Contour plots of conditional and indicator correlograms for Aug (upper) and Nov (lower).

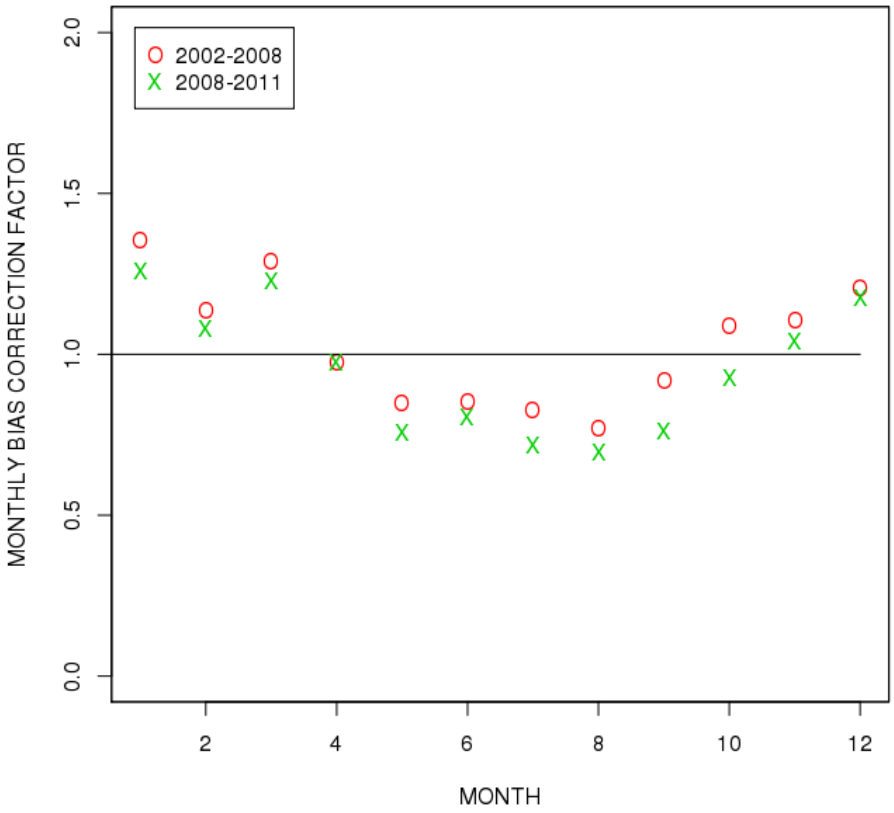

Fig. 3. Monthly bias correction factor for radar-only QPE.

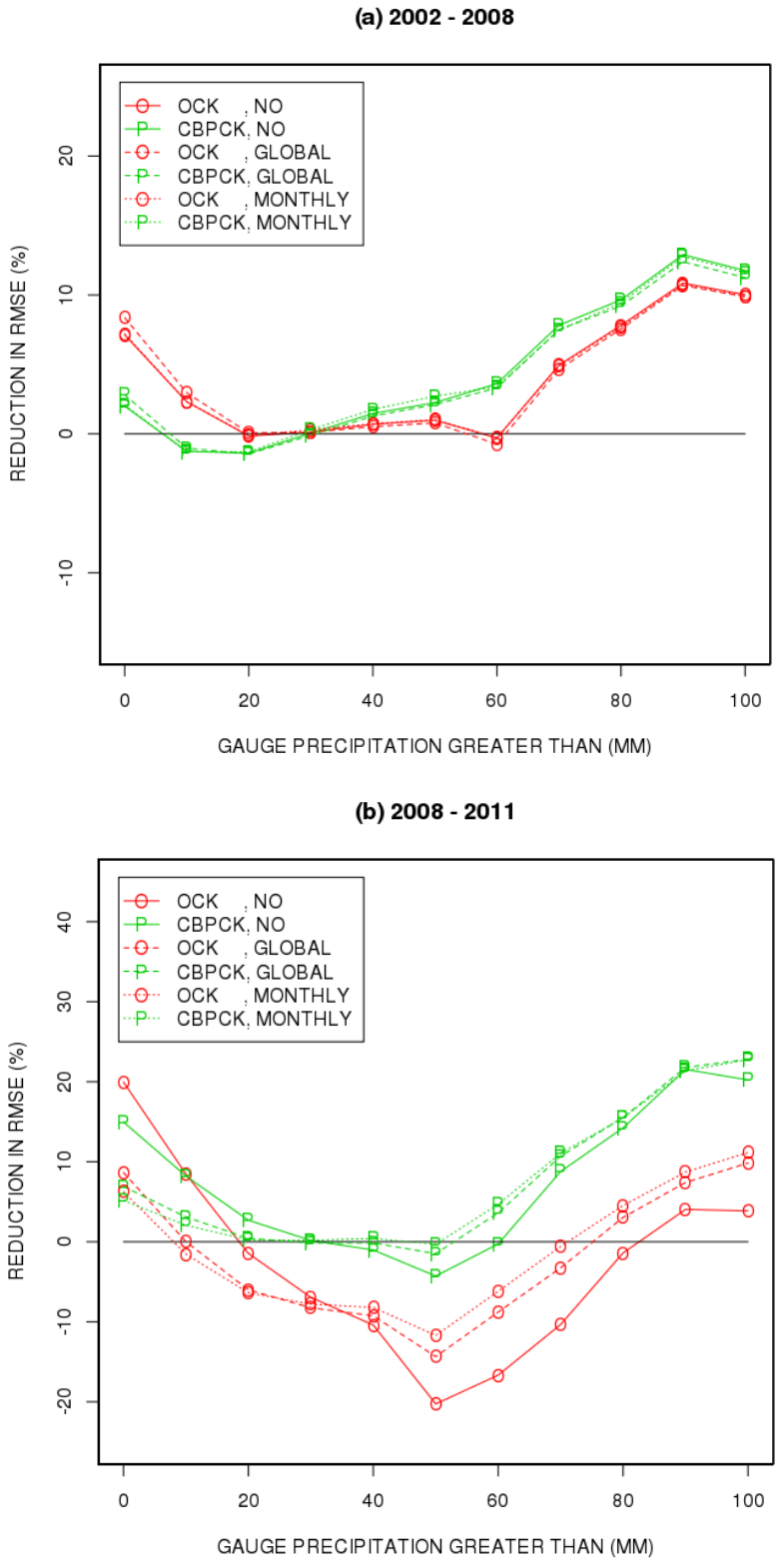

Fig. 4. Percent reduction in RMSE by OCK and CBPCK over RO without bias correction and with global and monthly bias correction.

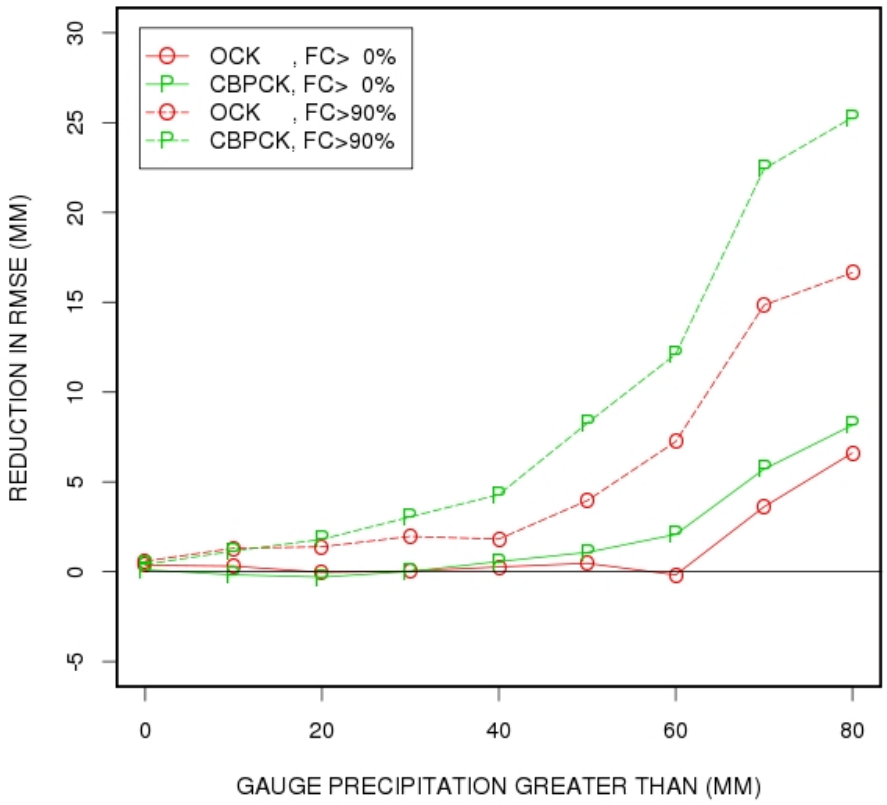

Fig. 5. Reduction in RMSE by CBPCK and OCK over RO (2002-2008).

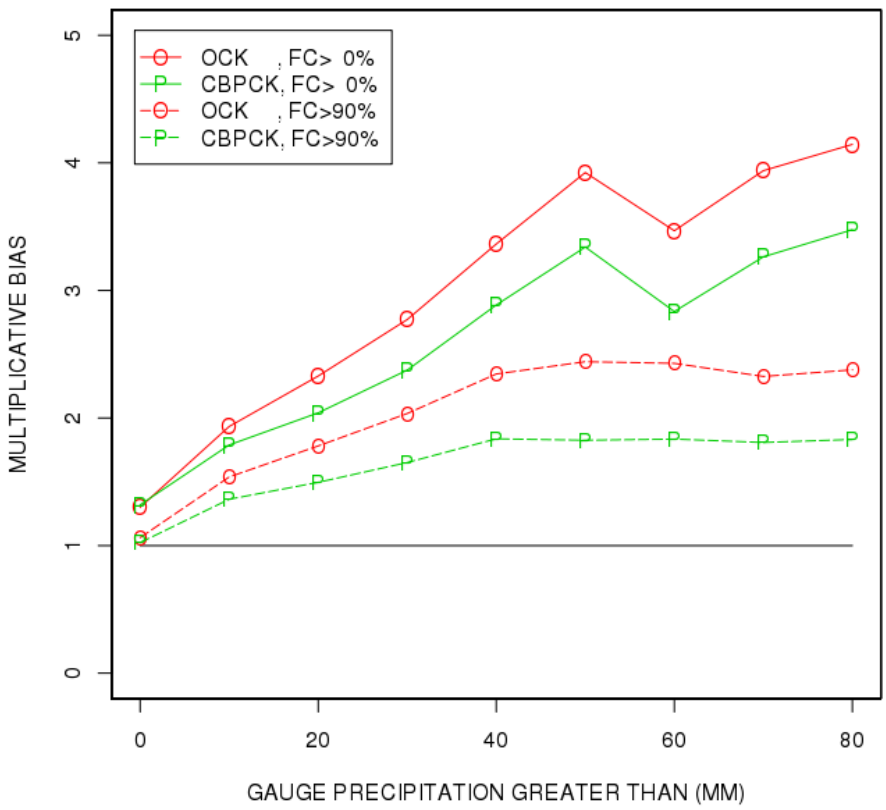

Fig. 6. Multiplicative bias (y-axis) of the precipitation estimate conditional on verifying amount exceeding the threshold (x-axis) for FC > 0 (solid line) and for FC > 0.9 (dashed line) (2002-2008).

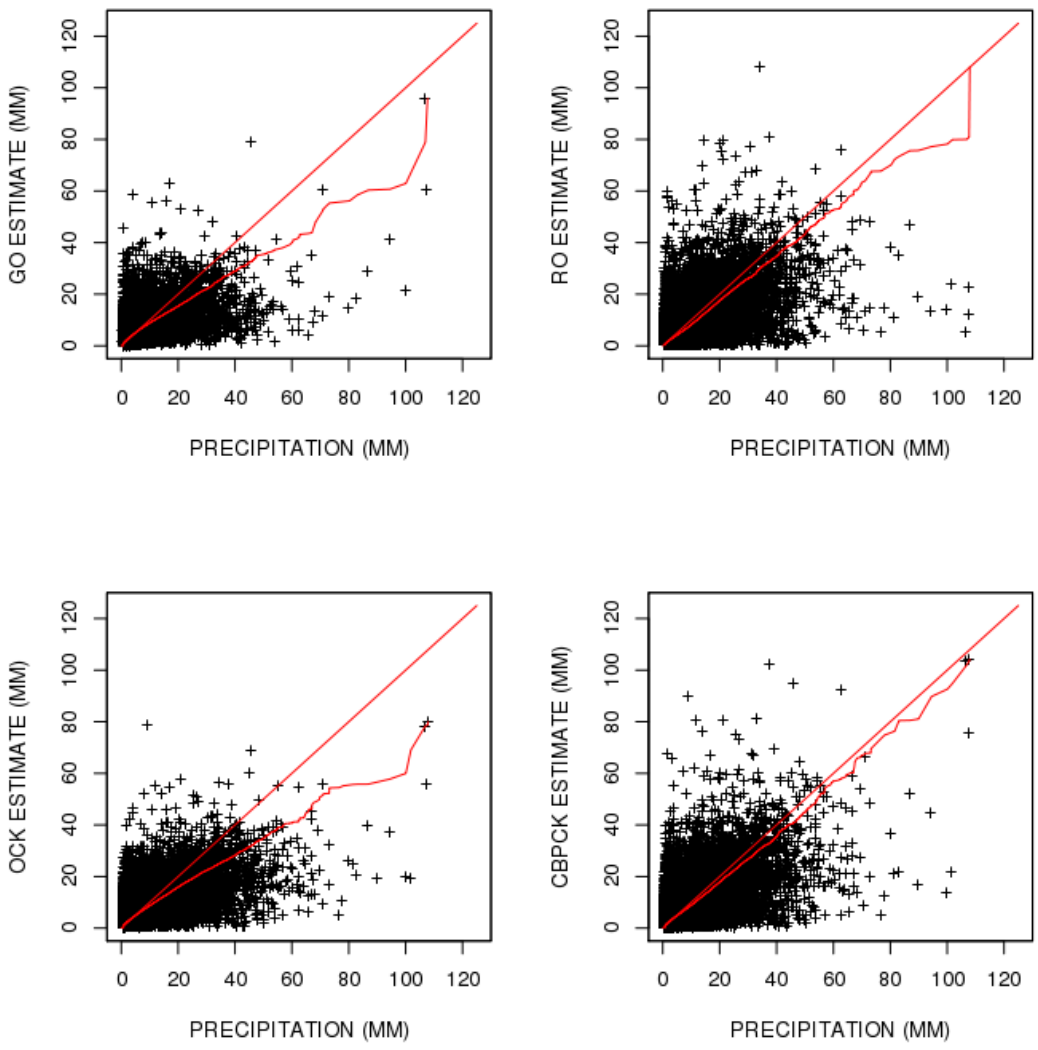

Fig. 7. Scatter and QQ plots of the truth vs. the hourly GO, RO, OCK and CBPCK estimates when FC exceeds 0.9 (2002-2008).

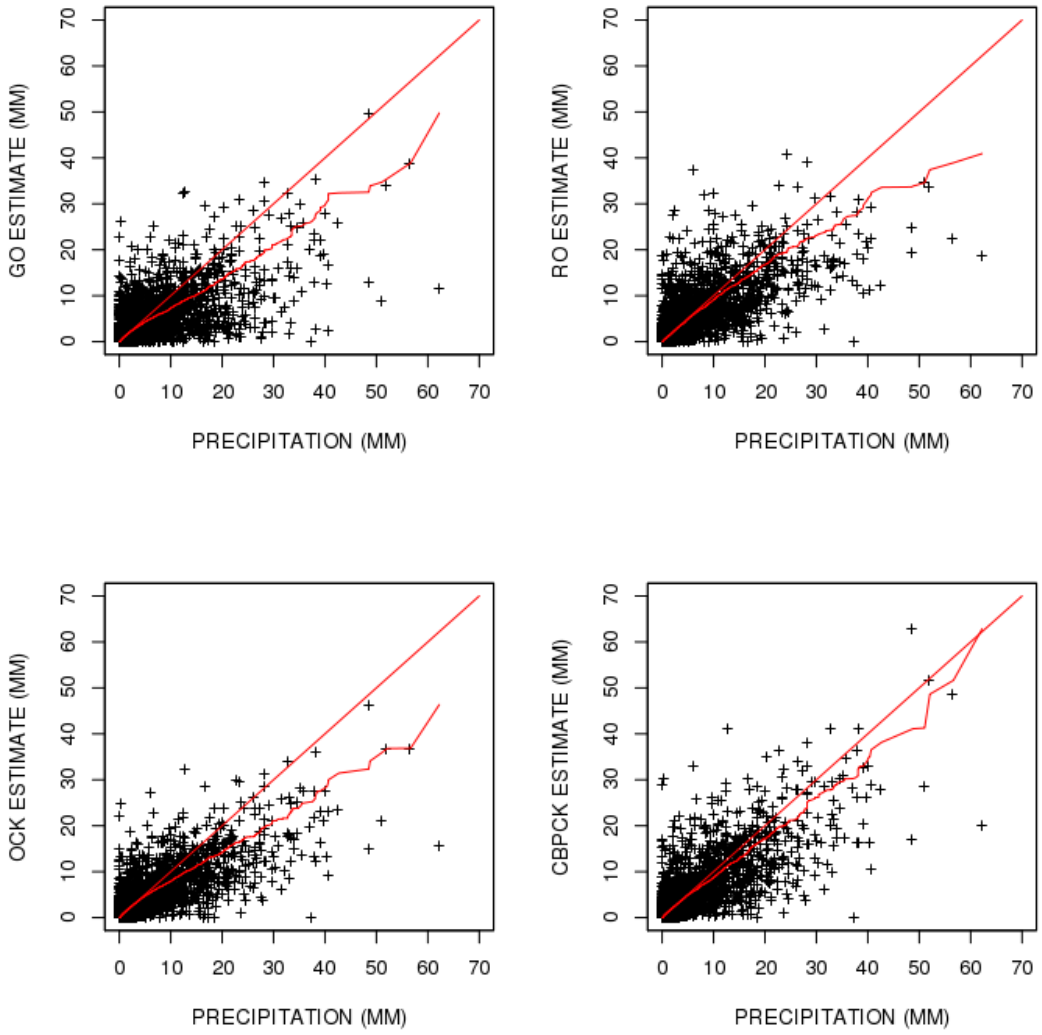

Fig. 8. Scatter and QQ plots of the truth vs. the hourly estimates for Apr 2008.

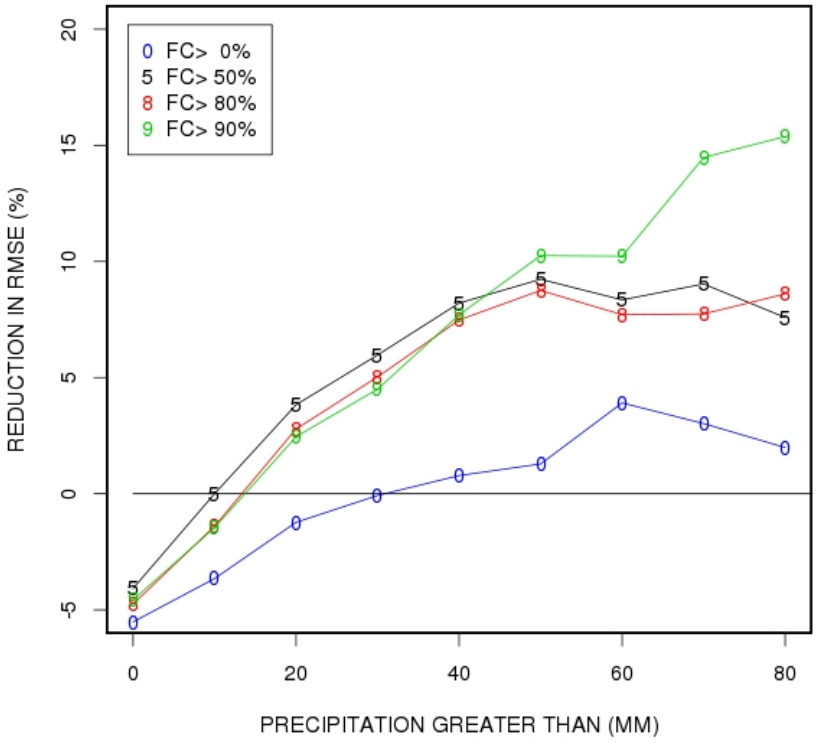

Fig. 9. Percent reduction in RMSE as a function of the minimum FC over the ungauged location by CBPCK over OCK (2002-2008).

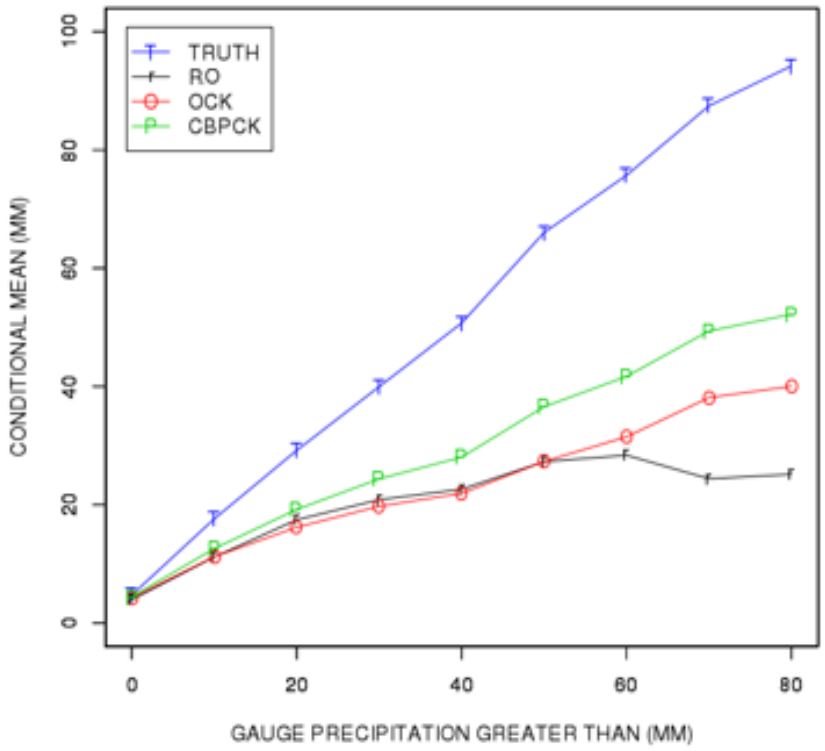

Fig. 10. Conditional mean of the gauge (identified as "TRUTH"), RO, OCK and CBPCK estimates for FC > 0.9 (2002-2008).

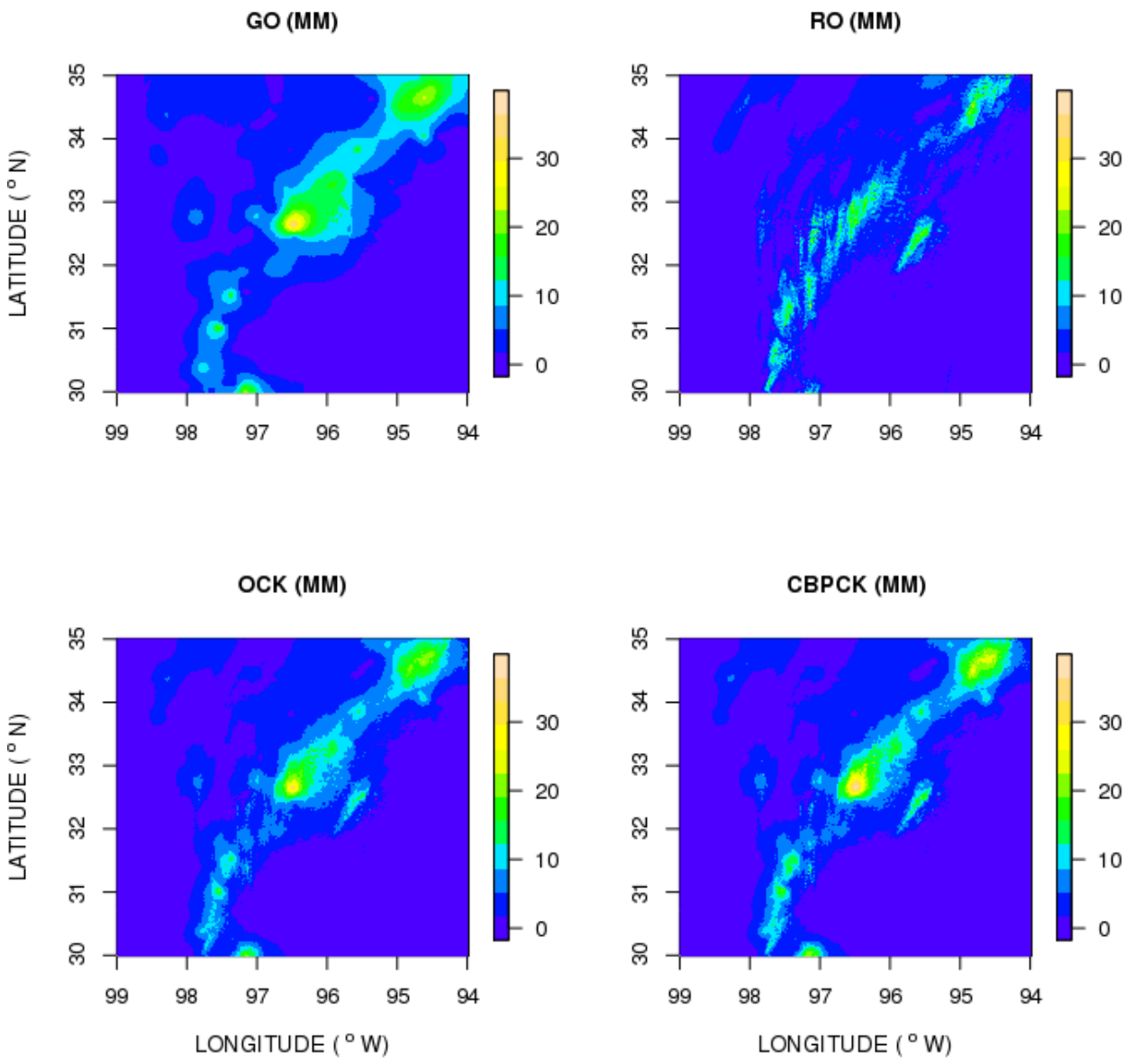

Fig. 11. Example fields of hourly precipitation from GO (upper-left), RO (upper-right), OCK (lower-left) and CBPCK (lower-right) valid at 9 pm Mar 18, 2008.

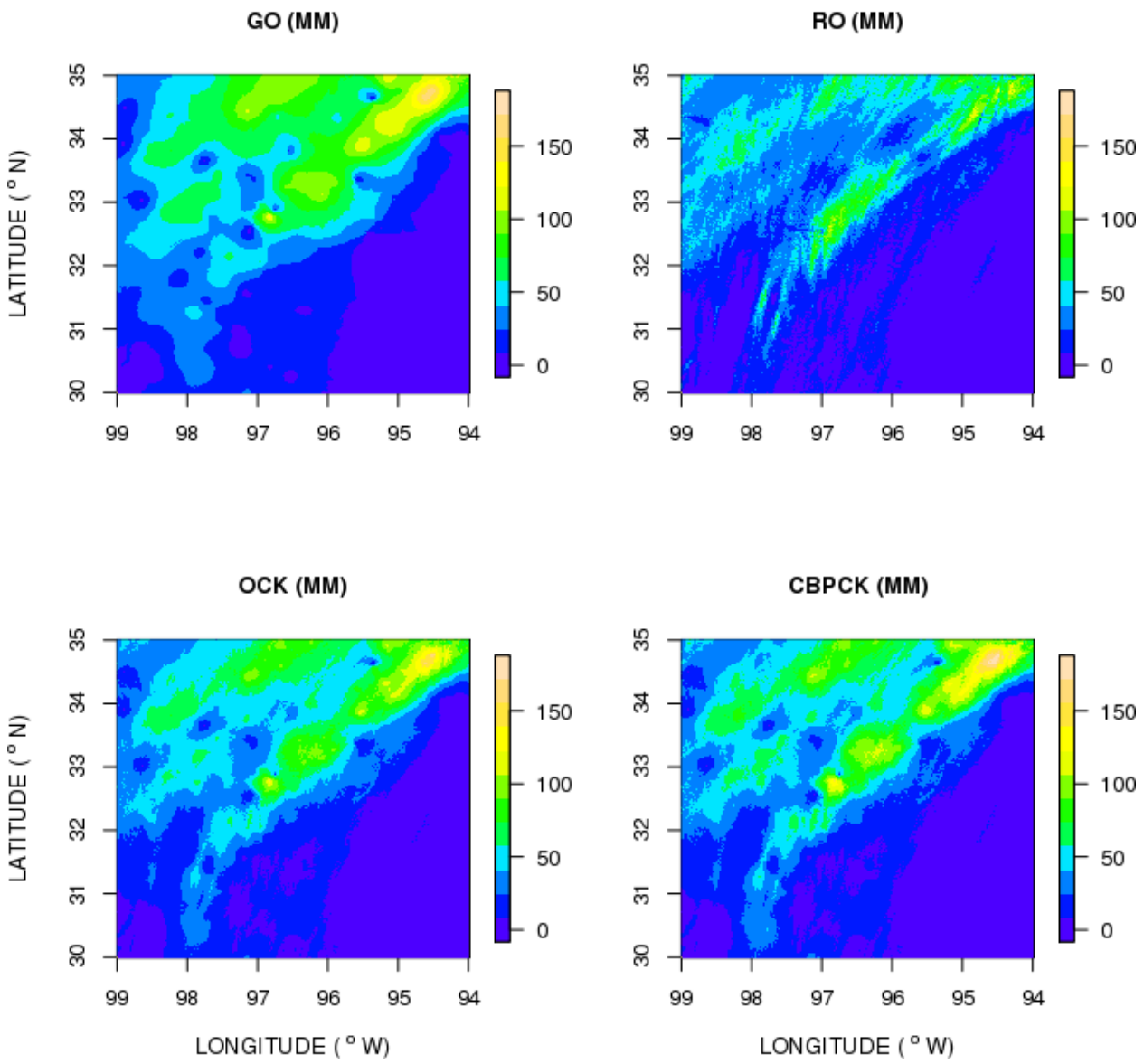

Fig. 12. Example fields of daily precipitation from GO (upper-left), RO (upper-right), OCK (lower-left) and CBPCK (lower-right) for Mar 18, 2008.

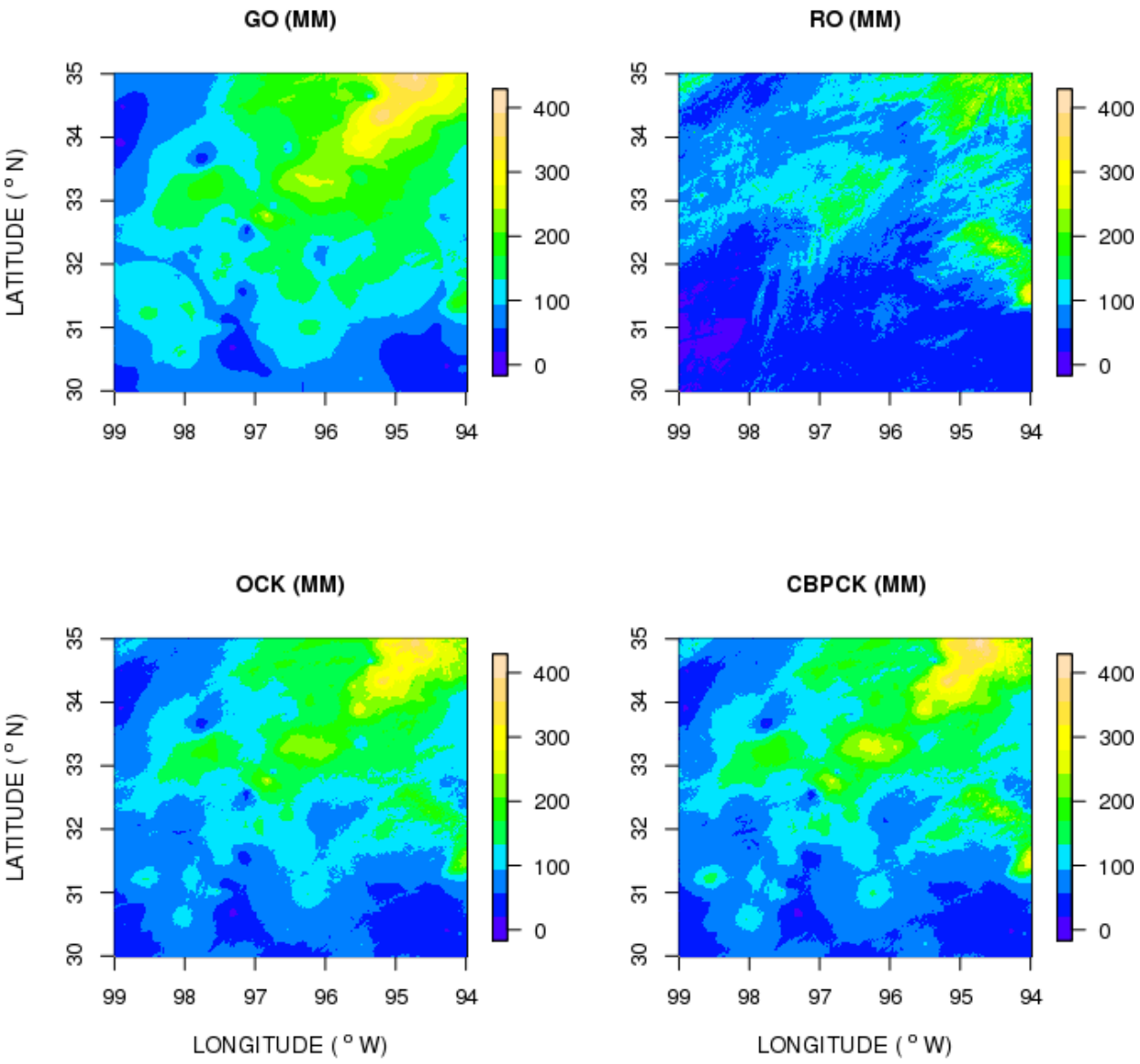

Fig. 13. Example fields of monthly precipitation from GO (upper-left), RO (upper-right), OCK (lower-left) and CBPCK (lower-right) for Mar 2008.

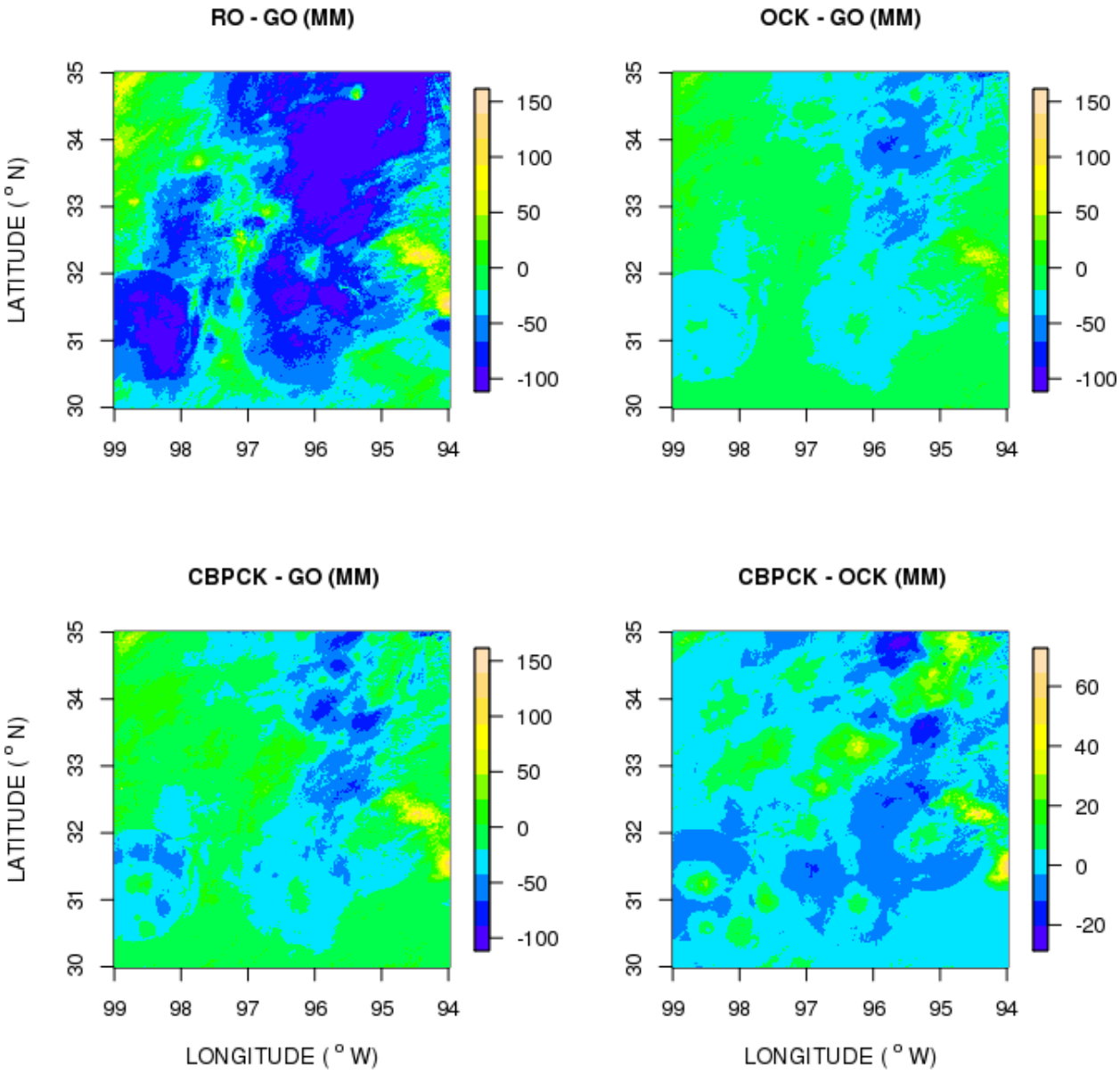

Fig. 14. Differences in monthly precipitation maps for Mar 2008 between the two estimation techniques shown in the figure title among GO, RO, OCK and CBPCK.

Table 1. Conditional and indicator correlogram model for each month.

Month	Model	Conditional Correlogram				Indicator Correlogram			
		Relative Nugget Effect	Range (Km)			Relative Nugget Effect	Range (Km)		
			Average	Minimum	Maximum		Average	Minimum	Maximum
Jan	ex	0.03	51.3	38.1	81.7	0.17	97.5	85.2	105.5
Feb	ex	0.03	47.4	31.9	71.3	0.15	94.9	82.7	107.9
Mar	ex	0.01	42.8	30.6	63.5	0.16	92.5	84.3	101.2
Apr	ex	0	58.9	33.8	127.2	0.15	97.4	91.2	105.6
May	ex	0	43.2	31.9	60.1	0.15	96.7	91.7	101.5
Jun	ex	0	36	29.4	45.5	0.19	82.5	78.1	88.2
Jul	ex	0.01	27.1	23	34	0.22	57.3	54.7	59
Aug	ex	0.01	27.6	24.2	33	0.21	66.2	60.3	70.6
Sep	ex	0.01	38.6	35.3	42.5	0.19	70.5	65.3	74
Oct	ex	0	59	40.3	81.7	0.16	97.2	91.4	101.4
Nov	ex	0	52.4	30.3	98.3	0.16	81.4	73.6	88.9
Dec	ex	0.04	43.2	31.5	68.4	0.18	94.3	86.8	103.9

* ex: exponential